REPORT DOCUMENTATION PAGE

Form Approved
OMB NO. 0704-0188

1. AGENCY USE ONLY (Leave Blank)	2. REPORT DATE	3. REPORT TYPE AND DATES COVERED
	2/4/2003	~~Interim, 1/1/02-07/31/02~~ Final 01 Jul 98 - 31 Jul 02

4. TITLE AND SUBTITLE	5. FUNDING NUMBERS
Defects in SiC Single Crystals and Their Influence on Device Performance	ARO Proposal #: 37560-MS
6. AUTHOR(S)	
Prof. Michael Dudley	
7. PERFORMING ORGANIZATION NAME(S) AND ADDRESS(ES)	8. PERFORMING ORGANIZATION REPORT NUMBER
Dept. of Materials Science & Engineering (Research Foundation of SUNY) State University of New York at Stony Brook NY 11794-2275	
9. SPONSORING / MONITORING AGENCY NAME(S) AND ADDRESS(ES)	10. SPONSORING / MONITORING AGENCY REPORT NUMBER
U. S. Army Research Office P.O. Box 12211 Research Triangle Park, NC 27709-2211	DAAG55-98-1-0392 37560.10.-MS

11. SUPPLEMENTARY NOTES

The views, opinions and/or findings contained in this report are those of the author(s) and should not be construed as an official Department of the Army position, policy or decision, unless so designated by other documentation.

12 a. DISTRIBUTION / AVAILABILITY STATEMENT	12 b. DISTRIBUTION CODE
Approved for public release; distribution unlimited.	

13. ABSTRACT (Maximum 200 words)

This extensive program of research aims to apply the techniques of Synchrotron White Beam X-ray Topography (SWBXT), Nomarski Optical Microscopy, Scanning Electron Microscopy, Transmission Electron Microscopy (TEM), and I-V Characteristic Probing to the detailed analysis of defect structures in SiC Single Crystals of various polytypes, and to determine how these defect structures can influence the performance of various kinds of device manufactures therefrom. Results obtained so far indicate that devices without screw dislocations exhibited excellent characteristics, with no detectable leakage current prior to breakdown, a sharp breakdown I-V knee, and no visible concentration of breakdown current. In contrast, devices that contained at least one elementary screw dislocation exhibited a 5% to 35% reduction in breakdown voltage, a softer breakdown I-V knee, and visible microplasmas at the sites of the screw dislocations. In addition a new strategy for preparing defect free 3C epilayers on 4H substrates was investigated. The success of this strategy was assessed using SWBXT,and results obtained to date reveal that high quality, poytype controlled 3C could be grown. The scope of the project was modified to encompass parallel studies of the influence of defect microstructure on the performance of resonators made from single crystals of the novel piezoelectric materials Langasite, Langanite and Langatate. Early results have indicated the presence of growth striations, dislocations and precipitates. The influence of these defects on device performance is being systematically studied.

14. SUBJECT TERMS	15. NUMBER OF PAGES
	16. PRICE CODE

17. SECURITY CLASSIFICATION OR REPORT	18. SECURITY CLASSIFICATION ON THIS PAGE	19. SECURITY CLASSIFICATION OF ABSTRACT	20. LIMITATION OF ABSTRACT
UNCLASSIFIED	**UNCLASSIFIED**	**UNCLASSIFIED**	**UL**

NSN 7540-01-280-5500

Standard Form 298 (Rev.2-89)
Prescribed by ANSI Std. 239-18
298-102

GENERAL INSTRUCTIONS FOR COMPLETING SF 298

The Report Documentation Page (RDP) is used for announcing and cataloging reports. It is important that this information be consistent with the rest of the report, particularly the cover and title page. Instructions for filling in each block of the form follow. It is important to ***stay within the lines*** to meet ***optical scanning requirements.***

Block 1. Agency Use Only (Leave blank)

Block 2. Report Date. Full publication date including day, month, and year, if available (e.g. 1 Jan 88). Must cite at least year.

Block 3. Type of Report and Dates Covered. State whether report is interim, final, etc. If applicable enter inclusive report dates (e.g. 10 Jun 87 - 30 Jun 88).

Block 4. Title and Subtitle. A title is taken from the part of the report that provides the most meaningful and complete information. When a report is prepared in more than one volume, repeat the primary title, and volume number, and include subtitle for the specific volume. On classified documents enter the title classification in parentheses.

Block 5. Funding Numbers. To include contract and grant numbers; may include program element number(s) project number(s), task number(s), and work unit number(s). Use the following labels:

C - Contract	**PR** - Project
G - Grant	**TA** - Task
PE - Program Element	**WU** - Work Unit Accession No.

Block 6. Author(s). Name(s) of person(s) responsible for writing the report, performing the research, or credited with the content of the report. If editor or compiler, this should follow the name(s).

Block 7. Performing Organization Name(s) and Address(es). Self-explanatory.

Block 8. Performing Organization Report Number. Enter the unique alphanumeric report number(s) assigned by the organization performing the report.

Block 9. Sponsoring/Monitoring Agency Name(s) and Address(es) Self-explanatory.

Block 10. Sponsoring/Monitoring Agency Report Number. (*if known)*

Block 11. Supplementary Notes. Enter information not included elsewhere such as; prepared in cooperation with....; Trans. of...; To be published in.... When a report is revised, include a statement whether the new report supersedes or supplements the older report.

Block 12a. Distribution/Availability Statement. Denotes public availability or limitations. Cite any availability to the public. Enter additional limitations or special markings in all capitals (e.g. NORFORN, REL, ITAR).

- **DOD** - See DoDD 4230.25, "Distribution Statements on Technical Documents."
- **DOE** - See authorities.
- **NASA** - See Handbook NHB 2200.2.
- **NTIS** - Leave blank.

Block 12b. Distribution Code.

- **DOD** - Leave Blank
- **DOE** - Enter DOE distribution categories from the Standard Distribution for unclassified Scientific and Technical Reports
- **NASA** - Leave Blank.
- **NTIS** - Leave Blank.

Block 13. Abstract. Include a brief (*Maximum 200 words)* factual summary of the most significant information contained in the report.

Block 14. Subject Terms. Keywords or phrases identifying major subject in the report.

Block 15. Number of Pages. Enter the total number of pages.

Block 16. Price Code. Enter appropriate price code (NTIS *only*).

Block 17. - 19. Security Classifications. Self-explanatory. Enter U.S. Security Regulations (i.e., UNCLASSIFIED). If form contains classified information, stamp classification on the top and bottom of the page.

Block 20. Limitation of Abstract. This block must be completed to assign a limitation to the abstract. Enter either UL (Unlimited) or SAR (same as report). An entry in this block is necessary if the abstract is to be limited. If blank, the abstract is assumed to be unlimited.

MASTER COPY: PLEASE KEEP THIS "MEMORANDUM OF TRANSMITTAL" BLANK FOR REPRODUCTION PURPOSES. WHEN REPORTS ARE GENERATED UNDER THE ARÒ SPONSORSHIP, FORWARD A COMPLETED COPY OF THIS FORM WITH EACH REPORT SHIPMENT TO THE ARO. THIS WILL ASSURE PROPER IDENTIFICATION. NOT TO BE USED FOR INTERIM PROGRESS REPORTS; SEE PAGE 2 FOR INTERIM PROGRESS REPORT INSTRUCTIONS.

MEMORANDUM OF TRANSMITTAL

U.S. Army Research Office
ATTN: AMSRL-RO-RI (Hall)
P.O. Box 12211
Research Triangle Park, NC 27709-2211

☐ Reprint (Orig + 2 copies)
☐ Technical Report (Orig + 2 copies)
☐ Manuscript (1 copy)
☒ Final Progress Report (Orig + 2 copies)
☐ Related Materials, Abstracts, Theses (1 copy)

CONTRACT/GRANT NUMBER: DAAG55-98-1-0392

REPORT TITLE: Defects in SiC Crystals and Their Influence on Device Performance

is forwarded for your information.

SUBMITTED FOR PUBLICATION TO (applicable only if report is manuscript):

Sincerely,

Richard Hall

TABLE OF CONTENTS

LIST OF REFEREED MANUSCRIPTS

The following manuscripts have either been submitted or published under ARO sponsorship during this reporting period:

1. W. M. Vetter and M. Dudley, "X-Ray Topographic Dislocation Contrast Visible in Reflections Orthogonal to the Burgers Vectors of Axial Screw Dislocations in Hexagonal Silicon Carbide", **J. Appl. Cryst., 34,** 20-26, (2001).

2. X. R. Huang, M. Dudley and J. Y. Zhao, "Forbidden X-ray wavefields of three-beam Bragg reflections from thick crystals", **Acta Cryst. A57,** 68-75, (2001).

3. M. Dudley, X.R. Huang, W.M. Vetter, and G. Dhanaraj, "Synchrotron White Beam X-ray Topography Characterization of Defects in Technologically Important SiC and InP Single Crystals", in "Crystal Growth and Characterization: Proceedings of International Workshop on the Preparation and Characterization of Technologically Important Single Crystals", S.K. Gupta, S.K. Halder, and G. Bhagavannarayana (Eds.), National; Physical Laboratory New Delhi, Feb. 26-28, 2001, pp. 44-51, (2001).

4. V. Prasad, Q.-S. Chen, H. Zhang, and M. Dudley, "Role of Modeling in Process and System Devlopment for Crystal Growth", in "Crystal Growth and Characterization: Proceedings of International Workshop on the Preparation and Characterization of

Technologically Important Single Crystals", S.K. Gupta, S.K. Halder, and G. Bhagavannarayana (Eds.), National; Physical Laboratory New Delhi, Feb. 26-28, 2001, pp. 95-102, (2001).

5. E.K. Sanchez, J. Liu, W.M. Vetter, M. Dudley, R. Bertke. W.C. Mitchel, and M. Skowronski, " Effect of Surface Finish on the Dislocation Density in Sublimation Grown SiC Layers", in "SiC - Materials, Processing and Devices", **Mat. Res. Soc. Symp. Proc., 640**, H1.3.1-H1.3.6, (2001).

6. S.E. Saddow, G. Melnychuk, M. Mynbaeva, I. Nikitina, W.M. Vetter, L. Jin, M. Dudley, M. Shamsuzzoha, V. Dmitriev, and C.E.C. Wood, "Structural Characterization of SiC Epitaxial LayersGrown on Porous SiC Substrates", in "SiC - Materials, Processing and Devices", **Mat. Res. Soc. Symp. Proc., 640**, H2.7.1-H2.7.6, (2001).

7. W. M. Vetter, W. Huang, P. Neudeck, J. A. Powell, M. Dudley, "Synchrotron White-Beam Topographic Studies of 2H-SiC Crystals", **J. Cryst. Growth, 224**, 269-273, (2001).

8. T. A. Kuhr, E. K. Sanchez, M. Skowronski, W. M. Vetter and M. Dudley, "Hexagonal Voids and the Formation of Micropipes During SiC Sublimation Growth", **J. Appl. Phys., 89**, 4625-4630, (2001).

9. J.C. Rojo, G.A. Slack, K. Morgan, B. Raghothamachar, M. Dudley, and L.J. Schowalter, " Report on the Growth of Bulk Aluminum Nitride and Susequent Substrate Preparation", **J. Cryst. Growth, 231**, 317-321, (2001).

10. W. M. Vetter and M. Dudley, "Transmission Electron Microscopy Studies of Dislocations in Physical-Vapour-Transport-Grown Silicon Carbide", **Phil. Mag., A81,** 2885-2902. (2001).

11. W. M. Vetter and M. Dudley, Partial Dislocations in the X-ray Topography of As-Grown Hexagonal Silicon Carbide Crystals. **Mater. Sci. Eng., B87**, 173, (2001).

12. E.K. Sanchez, S. Ha, J. Grim, M. Skowronski, W.M. Vetter, M. Dudley, R. Bertke and W.C. Mitchel, "Assessment of Polishing-Related Surface Damage in Silicon Carbide", **J. Electrochem. Soc., 149**, G131, (2002).

13. M. Dudley, B. Raghothamachar, H. Chen, A.J. Khan, S. Tiddrow, and C. Fazi, "Characterization of Defect and Strain Configurations in Langanite and Langatate Single Crystals using Synchrotron White Beam X-ray Topography and Assessment of their Influence on Resonator Performance" in Proceedings of 14th European Frequency and Time Forum, Turin Italy, March 14-16, 2000, in Press, (2001).

14. M. Dudley, B. Raghothamachar, H. Chen, W. Johnson, S. Tiddrow, A. Khan, and C. Fazi, "Diagnostic Synchrotron Topographic Imaging of Striations and other Defects

in Langatate and Langanite Single Crystals and Assessment of their Influence on Resonator Performance" in Proceedings of 15th European Frequency and Time Forum, Neuchatel, Switzerland, March 6-8, 2001, FSRM (Swiss Foundation for Research in Microtechnology), Neuchatel, Switzerland, (2001), pp.284-288.

15. W. M. Vetter, T. Gallagher and M. Dudley, "Synchrotron White-Beam X-Ray Topography of Ribonuclease S Crystals", **Acta Cryst., D58,** 579, (2002).

16. E.K. Sanchez, J.Q. Liu, M. De Graef, M. Skowronski, W.M. Vetter, and M. Dudley, "Nucleation of Threading Dislocations in Sublimation Grown Silicon Carbide", **J. Appl. Phys., 91**, 1143-1148, (2002).

17. M. Dudley, W.M. Vetter, and P.G. Neudeck, "Polytype Identification in Heteroepitaxial 3C-SiC Grown on 4H-SiC Mesas Using Synchrotron White Beam X-ray Topography", **J. Cryst. Growth, 240**, 22, (2002).

18. M. Dudley, W.M. Vetter, P.G. Neudeck, and J.A. Powell, "Polytype Identification and Mapping in Hetroepitaxial Growth of 3C on Atomically Flat 4H-SiC Mesas Using Synchrotron White Beam X-ray Topography," in *Silicon Carbide, III-Nitrides, and Related Materials 2001,* S. Yoshida, S. Nishino, H. Harima, and T. Kimoto (Eds.), **Materials Science Forum, 389-393**, 391-394, Trans Tech Publications, Switzerland, (2002).

19. P.G. Neudeck, J.A. Powell, A. Trunek, X.R. Huang, and M. Dudley, "Growth of defect-Free 3C-SiC on 4H- and 6H-SiC Mesas Using Step-Free Surface Heteroepitaxy", Homoepitaxial "Web Growth" of SiC to Terminate c-axis Screw Dislocations and Enlarge Step-Free Surfaces", in *Silicon Carbide, III-Nitrides, and Related Materials 2001,* S. Yoshida, S. Nishino, H. Harima, and T. Kimoto (Eds.), **Materials Science Forum, 389-393**, 311-314, Trans Tech Publications, Switzerland, (2002).

20. P. G. Neudeck, J.A. Powell, A. Trunek, D. Spry, G.M. Beheim, E. Benavage, P. Abel, W.M. Vetter, and M. Dudley, "Homoepitaxial "Web Growth" of SiC to Terminate c-axis Screw Dislocations and Enlarge Step-Free Surfaces", in *Silicon Carbide, III-Nitrides, and Related Materials 2001,* S. Yoshida, S. Nishino, H. Harima, and T. Kimoto (Eds.), **Materials Science Forum, 389-393**, 251-254, Trans Tech Publications, Switzerland, (2002).

21. S. Ha, W.M. Vetter, M. Dudley and M. Skowronski, "A Simple Mapping Method for Elementary Screw Dislocations in Homoepitaxial SiC Layers", in *Silicon Carbide, III-Nitrides, and Related Materials 2001,* S. Yoshida, S. Nishino, H. Harima, and T. Kimoto (Eds.), **Materials Science Forum, 389-393**, 443-446, Trans Tech Publications, Switzerland, (2002).

22. B.J. Skromme, K.C. Palle, C.D. Poweleit, L.R. Bryant, W.M. Vetter, M. Dudley, K. Moore, and T. Gehoski, "Oxidation-Induced Crystallographic Transformation in

Heavily N-Doped 4H-SiC Wafers", in *Silicon Carbide, III-Nitrides, and Related Materials 2001,* S. Yoshida, S. Nishino, H. Harima, and T. Kimoto (Eds.), **Materials Science Forum, 389-393,** 455-458, Trans Tech Publications, Switzerland, (2002).

23. W.M. Vetter, H. Totsuka, M. Dudley, and B. Kahr, "The Perfection and Defect Structure of Organic Hourglass Inclusion K_2SO_4 Crystals", to Appear in **J. Cryst. Growth**, (2002).

24. P.G. Neudeck, J.A. Powell, G.M. Beheim, E.L. Benavage, P.B. Abel, A.J. Trunek, D.J. Spry, M. Dudley, and W.M. Vetter, "Enlargement of Step-Free SiC Surfaces by Homoepitaxial Web-Growth of Thin SiC Cantilevers, submitted to **J. Appl. Phys.,** (2002).

25. S. Ha, M. Skowronski, W.M. Vetter, and M. Dudley, "Basal Plane Slip and Formation of Mixed-Tilt Boundaries, in Sublimation-Grown Hexagonal Polytype Silicon Carbide Single Crystals", **J. Appl. Phys., 92,** 778-785, (2002).

26. P.G. Neudeck, J.A. Powell, G.M. Beheim, E.L. Benavage, P.B. Abel, A.J. Trunek, D.J. Spry, M. Dudley, and W.M. Vetter, "Enlargement of Step-Free SiC Surfaces by Homoepitaxial Web-Growth of Thin SiC Cantilevers", **J. Appl. Phys., 92,** 2391,-2400, (2002).

27. M. Skowronski, J.Q. Liu, W.M. Vetter, M. Dudley, C. Hallin, and H. Lendenmann, "Recombination-Enhanced Defect Motion in Forward-Biased 4H-SiC p-n Diodes," **J. Appl. Phys., 92,** 4699-4704, (2002).

LIST OF PRESENTATIONS

1. International Workshop on Preparation and Characterization of Technologically Important Single Crystals, National Physical Laboratory, New Delhi, India, February 26-28, 2001: "Synchrotron White Beam X-ray Topography Characterization of Defects in Technologically Important SiC and InP Single Crystals" (Invited Lecture).

2. International Workshop on Preparation and Characterization of Technologically Important Single Crystals, National Physical Laboratory, New Delhi, India, February 26-28, 2001: "Role of Modeling in Process and System Development for Crystal Growth" (Oral presentation with V. Prasad, Q.-S. Chen, and H. Zhang – lecture presented by V. Prasad).

3. 15th European Frequency and Time Forum, Neuchatel, Switzerland, March 6-8, 2001, "Diagnostic Synchrotron X-Ray Topographic Imaging of Striations and Other

Defects in Langatate and Langanite Single Crystals and Assessment of Their Influence on Resonator Performance (Poster Presentation with C. Fazi, S. Tiddrow, W. Johnson, and A. Khan – Poster presented by C. Fazi).

4. Inter University Consortium, Indore, India, March 5, 2001: "Synchrotron White Beam X-ray Topography Characterization of Defects in SiC and InP Single Crystals" (Invited Lecture).

5. Department of Physics, Indian Institute of Science, Bangalore, India, March 8, 2001: "Characterization of defects in SiC Single Crystals" (Invited Lecture).

6. Department of Physics, Anna University, Chennai, India, March 9, 2001: "Synchrotron White Beam X-ray Topography Characterization of Defects in SiC Single Crystals" (Invited Lecture).

7. Materials Science Center, Dept. of Nuclear Physics, University of Madras, Chennai, India, March 9, 2001: "Synchrotron White Beam X-ray Topography Characterization of Defects in SiC and InP Single Crystals" (Invited Lecture).

8. MURI Nitrides Kick-Off Meeting, Dept. of Materials Science & Engineering, North Carolina State University, Raleigh, NC, May 20-22, 2001: "SWBXT and HRTXD of Widebandgap Semiconductors" (Invited Lecture).

9. ONR Workshop on Challenges in Porous and Amorphous Widebandgap Semiconductors, Corner Brook, Newfoundland, Canada, June 10-14, 2001: "Synchrotron Topography Characterization of Porous Materials" (Invited Lecture).

10. ONR Workshop on Near Surface Effects in Semiconductor Substrates, Kodiak Island, Alaska, August 5-10, 2001: "Simultaneous Structural and Microstructural Analaysis of Polytype Distributions in 3C-SiC Epitaxial Films Grown on Atomically Flat 4H-SiC Mesas using Synchrotron White Beam X-ray Topography" (Invited Lecture).

11. Thirteenth American Conference on Crystal Growth and Epitaxy, Burlington, VT, August 12-16, 2001: "Polytype Identification in Heteroepitaxial 3C/4H SiC using Synchrotron White Beam X-ray Topography" (Invited Lecture).

12. International Conference on SiC and Related Materials 2001, Tsukuba, Japan, October 28-November 2, 2001: "Polytype Identification and Mapping in Hetroepitaxial Growth of 3C on Atomically Flat 4H-SiC Mesas Using Synchrotron White Beam X-ray Topography," (Lecture with W.M. Vetter, P.G. Neudeck, and J.A. Powell – Lecture Presented by P. Neudeck).

13. International Conference on SiC and Related Materials 2001, Tsukuba, Japan, October 28-November 2, 2001: "Growth of defect-Free 3C-SiC on 4H- and 6H-SiC Mesas Using Step-Free Surface Heteroepitaxy", Homoepitaxial "Web Growth" of

SiC to Terminate c-axis Screw Dislocations and Enlarge Step-Free Surfaces", (Lecture with P.G. Neudeck, J.A. Powell, A. Trunek, and X.R. Huang –Lecture Presented by P. Neudeck).

14. International Conference on SiC and Related Materials 2001, Tsukuba, Japan, October 28-November 2, 2001: "Homoepitaxial "Web Growth" of SiC to Terminate c-axis Screw Dislocations and Enlarge Step-Free Surfaces", (Lecture with P.G. Neudeck, J.A. Powell, A. Trunek, D. Spry, G.M. Beheim, E. Benavage, P. Abel, and W.M. Vetter – Lecture Presented by P. Neudeck).

15. International Conference on SiC and Related Materials 2001, Tsukuba, Japan, October 28-November 2, 2001: "A Simple Mapping Method for Elementary Screw Dislocations in Homoepitaxial SiC Layers", (Lecture with S. Ha, W.M. Vetter, and M. Skowronski – Lecture Presented by S. Ha).

16. International Conference on SiC and Related Materials 2001, Tsukuba, Japan, October 28-November 2, 2001: "Oxidation-Induced Crystallographic Transformation in Heavily N-Doped 4H-SiC Wafers", (Lecture with B.J. Skromme, K.C. Palle, C.D. Poweleit, L.R. Bryant, W.M. Vetter, K. Moore, and T. Gehoski – Lecture Presented by B.J. Skromme).

17. Los Alamos National Laboratory, Feb 19, 2002: "Synchrotron White Beam X-ray Topography and High Resolution Triple-Axis X-ray Diffraction Studies of Defects in SiC Substrates, Epilayers and Device Structures (Invited Lecture).

18. 7th International Workshop on Wide Bandgap III-Nitrides, Richmond, VA, March 10-14, 2002: "Synchrotron White Beam Topogrpahy Characterization of Physical Vapor Transport Grown AlN andf Ammonothermal GaN" (Lecture with B. Raghothamachar, W.M. Vetter, H. Zhang, R. Ma, Z. Sitar, R. Schlesser, and J.W. Kolis – Lecture Presented by M. Dudley).

19. 7th International Workshop on Wide Bandgap III-Nitrides, Richmond, VA, March 10-14, 2002: "Structural Characterization of Epitaxial Layers Grown on Porous SiC Substrates" (Poster with P. Gouma, B. Raghothamachar, J. Bie, S. Saddow, and M. Smith – Poster Presented by P. Gouma, B. Raghothamachar, J. Bie, and M. Dudley).

20. 1st Annual MURI Review for "An Integrated Approach to Bulk III-Nitride Crystal Growth ans Wafering", Cornell University, Ithaca, NY, April 25-26, (2002): "Synchrotron White Beam X-ray Topography Characterization of Ammonothermally Grown GaN" (Invited Lecture with B. Raghothamachar, W.M. Vetter, J.W. Kolis and E. Michaels – Lecture Presented by B. Raghothamachar).

21. 1st Annual MURI Review for "An Integrated Approach to Bulk III-Nitride Crystal Growth ans Wafering", Cornell University, Ithaca, NY, April 25-26, (2002): "Synchrotron White Beam X-ray Topography Characterization of Physical Vapor

Transport Grown AlN" (Invited Lecture with B. Raghothamachar, W.M. Vetter, Z. Sirat and R. Schlesser – Lecture Presented by B. Raghothamachar).

22. International Workshop on Bulk Nitride Semiconductors, Amazonas Brazil, May 18-23, 2002: "Synchrotron White Beam X-ray Topography Characterization of Physical Vapor Transport Grown AlN and Ammonothermal GaN" (Invited Lecture).

23. International Workshop on Challenges in Semi-Insulating Nitrides and SiC, Laugarvatn Iceland, July 14-18, 2002: "Sycnhrotron White Beam X-ray Topography Characterization of Semi-Insulating, Physical Vapor Transport Grown SiC and AlN " (Invited Lecture).

24. Wide Bandgap/II-VI Inc, Pine Brook. NJ, July 26, 2002: "Synchrotron White Beam X-ray Topography and High Resolution Triple-Axis X-ray Diffraction Studies of Defects in SiC Substrates, Epilayers and Device Structures", (Invited Lecture).

25. XIX Congress and General Assembly of International Union of Crystallography, Geneva, Switzerland, August 6-15, 2002: "Synchrotron White Beam X-ray Topography and High Resolution Triple-Axis X-ray Diffraction Studies of Defects in SiC Substrates, Epilayers and Device Structures", (Invited Lecture).

26. European Conference on SiC and Related Materials, Linkoping, Sweden, September 1-5, 2002: "Synchrotron White Beam X-ray Topography and High Resolution Triple-Axis X-ray Diffraction Studies of Defects in SiC Substrates, Epilayers and Devices", (Invited Lecture).

27. 6th Biennial Conference on High Resoultion Diffraction and Imaging (X-Top 2002), Grenoble/Aussois, France, September 10-14, 2002: "Contribution of X-ray Topography and High resolution X-ray Diffraction to the Study of Defects in SiC", (Invited Lecture).

28. 2nd Annual MURI Review for "An Integrated Approach to Bulk III-Nitride Crystal Growth and Wafering", Arizona State University, Tempe, AZ, November 18-19, (2002): "Synchrotron White Beam X-ray Topography Characterization of Ammonothermally Grown GaN" (Invited Lecture with B. Raghothamachar, W.M. Vetter, J.W. Kolis and E. Michaels – Lecture Presented by B. Raghothamachar).

29. 2nd Annual MURI Review for "An Integrated Approach to Bulk III-Nitride Crystal Growth ans Wafering", Arizona State University, Tempe, AZ, November 18-19, (2002): "Synchrotron White Beam X-ray Topography Characterization of Physical Vapor Transport Grown AlN" (Invited Lecture with B. Raghothamachar, W.M. Vetter, Z. Sitar and R. Schlesser – Lecture Presented by B. Raghothamachar).

30. Fall 2002 MRS Symposium on "Silicon Carbide – Materials, Processing, and Devices", Boston, MA, December 2-6, 2002: "Characterization of Porous SiC

Substrates and the Epilayer Structures Grown on Them" (Poster with J. Bai, P. Gouma, M. Mynbaeva, and S. Saddow – poster presented by J. Bai, P. Gouma, M. Mynbaeva, and S. Saddow).

31. Fall 2002 MRS Symposium on "Silicon Carbide – Materials, Processing, and Devices", Boston, MA, December 2-6, 2002: "Effects of Structural Defects on Diode Properties in 4H-SiC (Lecture with B.J. Skromme, K. Palle, H. Meidia, S. Mahajan, W.M. Vetter, K. Moore, S. Smith and T. Gehoski – Lecture presented by B.J. Skromme).

32. Fall 2002 MRS Symposium on "Silicon Carbide – Materials, Processing, and Devices", Boston, MA, December 2-6, 2002: Accurate Lattice Constant and Mismatch Measurements of SiC Heterostructures using Harmonic X-ray Reflections" (Lecture with X. Huang, P.G. Neudeck and J.A. Powell – Lecture presented by X. Huang).

SCIENTIFIC PERSONNEL AND HONORS/AWARDS/DEGREES

The following scientific personnel were supported by this project during this reporting period:

Senior Personnel: P.I., Prof. Michael Dudley

Postdoctoral Fellow: William M. Vetter

Graduate Students: Huaibin Chen

The following honors/awards/degrees were received during this reporting period:

REPORT OF INVENTIONS

None

SCIENTIFIC PROGRESS AND ACCOMPLISHMENTS:

This Final Progress Report is divided into two main sections: (1) SWBXT and HRTXD Studies of 3C, 4H and 6H SiC, and (2) SWBXT Studies of Langasite and other Langasite Structure Compounds.

1. SWBXT and HRTXD Studies of 3C, 6H and 4H SiC:

In the last reporting period, Synchrotron White Beam X-ray topographic images have continued to be recorded from 6H and 4H SiC substrates, substrates with epilayers grown on them, and epilayers with devices fabricated on them. The substrates for these samples were commercially available SiC wafers from a variety of sources, including Cree Research Inc., Advanced Technology Materials Inc., (ATMI) and Sterling Semiconductor. The bare substrate wafers studied are to be used as substrates to grow epitaxial layers to be subsequently used for device fabrication. Likewise those samples with just bare epilayers are to be subsequently used for device fabrication. For the case of those samples examined which have devices already fabricated on them the impact of elementary and larger screw dislocations on the reverse bias current-voltage (I-V) characteristics could be directly investigated. SWBXT images were recorded in the back-reflection, grazing-incidence or transmission geometry to reveal dislocations and other crystallographic defects as well as for polytype identification. Images obtained are similar to those presented in previous reports and are not reproduced here. However, new types of defects in SiC, such as specially configured partial dislocations, were identified and characterized. These defects provide new insights into SiC crystal growth and post-growth processes, and details are in preparation for publication.

In this report, we concentrate on the characterization of 3C SiC epilayers grown on atomically flat 4H and 6H SiC mesas using High Resolution Triple-axis X-ray Diffraction (HRTXD).

Polytype Identification in 3C/4H SiC

SiC is not only a promising substrate material for III-nitrides but 4H and 6H SiC have also attracted much attention as substrates for epitaxial growth of 3C SiC since the in-plane lattice mismatch for such heterostructures is almost negligible in the basal planes while the bandgap differs significantly across the interfaces. Unfortunately, 3C epilayers grown on 4H or 6H substrate generally contain high densities of defects including double-positioning boundaries and stacking faults. Threading SSDs in the substrate play a significant role in the formation of these defects. Firstly, SSDs cannot coherently propagate into the 3C epilayers due to the difference in stacking sequence and periodicity. Instead, the termination of SSDs at the interfaces induces other defects to compensate the Burgers vectors. Secondly but more significantly, the self-regenerating atomic steps (spirals) of SSDs widely spread on the entire substrate surface can cause more defects in the epilayer [1].

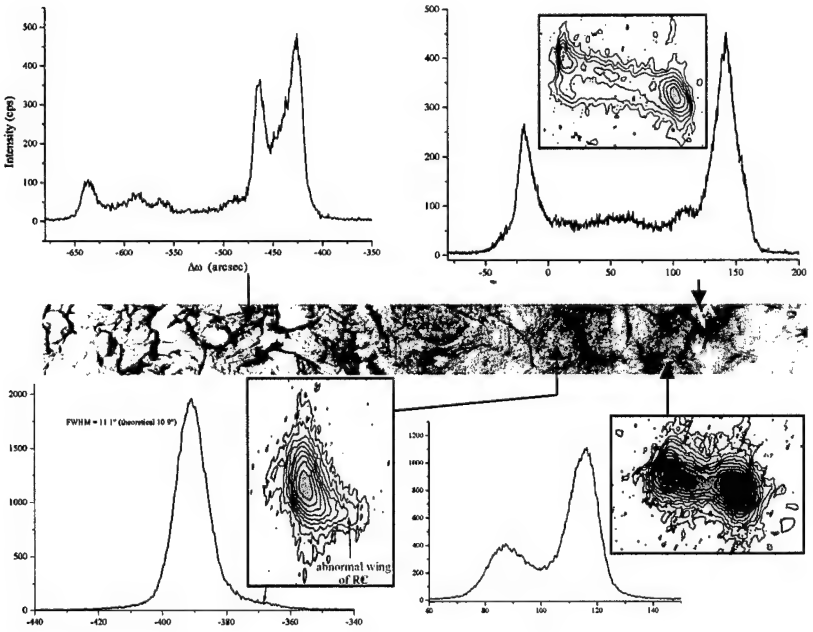

Fig. 1. Splitting of diffraction peaks as a consequence of small-angle boundaries and dislocations in a 4H-SiC crystal. The image in the middle is a back-reflection topograph showing the defects in the crystal. The arrows indicate the X-ray diffraction locations where the rocking curves were measured. The corresponding reciprocal maps indicate that the mulitple peaks are mainly associated with lattice misorientations rather than d-spacing variations. 0004 reflection. CuKα1 radiation. The Rocking curves and reciprocal maps were measured with a Bede D1 system with asymmetric monochromators (and analyzer).

It is worth mentioning that the existence of SSDs and small-angle boundaries in SiC substrates generally makes it difficult to solely use high-resolution X-ray diffraction (HRXRD) techniques to characterize epilayers grown on them because these defects themselves can give rise to multiple peaks in the rocking curves. Therefore, small-beam footprints are required for the HRXRD measurements. On the other hand, back-reflection topographs are of great help for one to direct the small X-ray beam to areas free of SSD and small-angle boundaries.

For example, figure 1 shows the small-beam (2 mm in diameter) rocking curves measured from different areas of a commercial 4H-SiC wafer. The corresponding SWBXT topograph clearly reveals that the well-shaped multiple diffraction peaks in the rocking curves are due to small-angle boundaries and dislocations. Using reciprocal space mapping, it was further revealed that these defects are mainly associated with misorientations of the local (0001) lattice planes since the spread of the diffraction spots in the reciprocal space maps is mainly along the horizontal directions. When the small X-ray beam was incident on nearly defect-free region (lower-left figure), a single diffraction peak was obtained, with the full width at half maxima (FWHM) of the rocking curve being 11.1 arcsec, very close to that of a perfect 4H-SiC crystal.

In characterization of 3C/4H or 3C/6H heterostructures, an important task is to verify the 3C structure of the epilayer since homoepitaxy or formation of other polytypes may easily occur if the heteroepitaxy conditions are not well controlled. Moreover, 3C

epilayers grown on the (0001) surface can have two twinned variants due to the symmetry decrease from a 6-fold rotation operation along [0001] in the substrate to a 3-fold one along [111] in the epilayers. SWBXT is capable of identifying the polytype and mapping the variant distribution since each SiC polytype or variant has its unique Laue pattern. Based on such a map, small-beam HRXRD measurements can subsequently be performed for selected areas.

As an example, here we briefly introduce a study recently carried out in our group for characterization of 3C/4H SiC heterostructures using SWBXT and HRXRD [2-4]. In this systematic research, the first task is to produce atomically flat 4H (and 6H) substrate surfaces for epitaxial growth of 3C films since the presence of atomic steps [resulted either from slight miscut or from the helical (0001) lattice planes around SSDs] on the surface means that different termination stacking sequences will be present side by side near a step so that if two-dimensional (2D) nucleation of 3C occurs, more than one variant will nucleate on a given mesa. The steps may also induce other high-density extended defects in the films, resulting in poor film quality and degraded device performance.

In order to remove the atomic steps, the 4H substrate surface was first patterned into an array of mesas by etching suitable trenches. Then if a mesa contains no SSD cores, its surface is either a flat or stepped surface, as represented by mesas A and B in Fig. 2, respectively. For stepped mesas, the step segments are isolated from the original step lines. The patterned surface was subsequently subjected to a homoepitaxial procedure designed to "grow out" all atomic steps based on the "step-flow" growth mechanism. Note that if the surface is not patterned, the homoepitaxial process can grow out only the steps arising from miscut, but not those from SSDs since the threading SSDs are continual sources of steps. Similarly, the mesas containing SSD cores are still stepped even after homoepitaxy, but the SSD core-free mesas can become atomically flat. If heteroepitiaxial growth is carried out afterwards, the flat mesas will experience uniform nucleation of one of the two 3C variants, resulting in high-quality 3C epilayers.

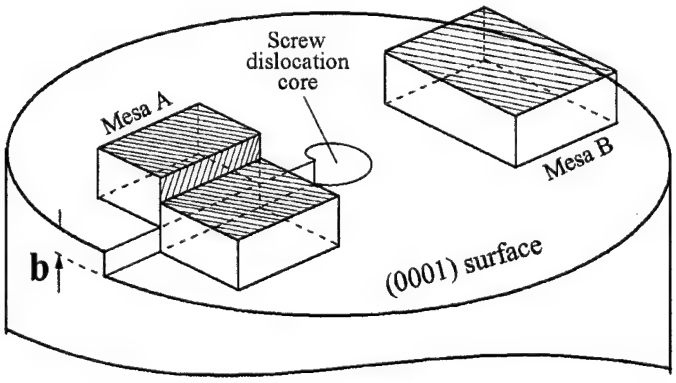

Fig. 2. Effects of mesas for disconnecting screw dislocation spirals on the (0001) SiC surface.

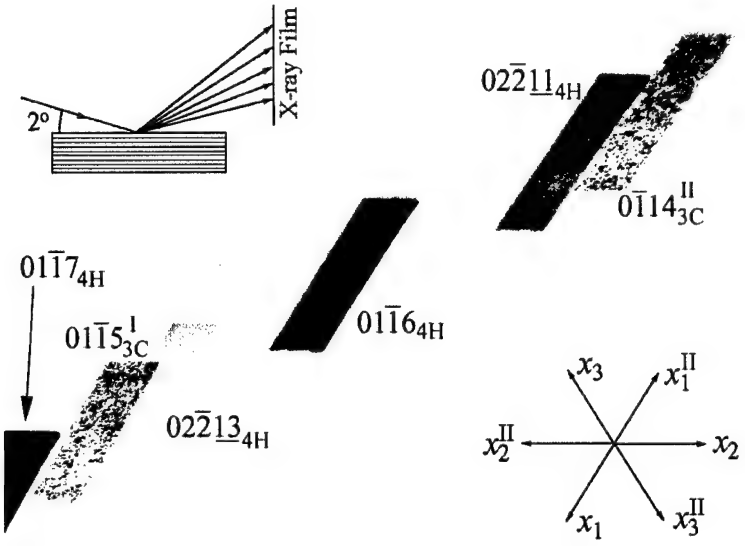

Fig. 3. Grazing-incidence SWBXT Laue pattern of 3C/4H SiC heterostructure. Upper-left inset illustrates diffraction geometry. (0001) surface. Incidence nearly along [-1010]. Lower-right inset shows the hexagonal coordinates used for indexing the diffraction spots. $x_1x_2x_3$ is the common coordinate system for 3C variant I and 4H while $x_1^{II}x_2^{II}x_3^{II}$ is related to $x_1x_2x_3$ by a 180° rotation operation for indexing 3C variant II.

SWBXT mapping of the distribution of the polytypes and their variants was carried out in grazing-incidence geometry. Due to the difference in crystal symmetry or orientation between the two 3C variants and the substrate, the Laue pattern consists of three sets of diffraction spots corresponding to the three structures, respectively. Then each 3C variant has several unique topographs that are not overlapped by reflections from the other variant or the substrate. Figure 3 shows a small portion of the Laue pattern taken from a 3C/4H SiC heterostructure under the grazing-incidence diffraction geometry. After correcting the projection distortion, one can superimpose two such topographs that are unique to the two 3C variants, respectively, onto the back-reflection topograph of the substrate to form a single figure showing the distribution of the 3C variants and the positions of the SSDs across the sample. Figure 4(a) shows an image that is made up of the superimposition of such three topographs. Interestingly, 3C epilayers were formed only on atomically flat mesas while they are almost completely absent in the trenches as well as on some mesas containing SSD cores.

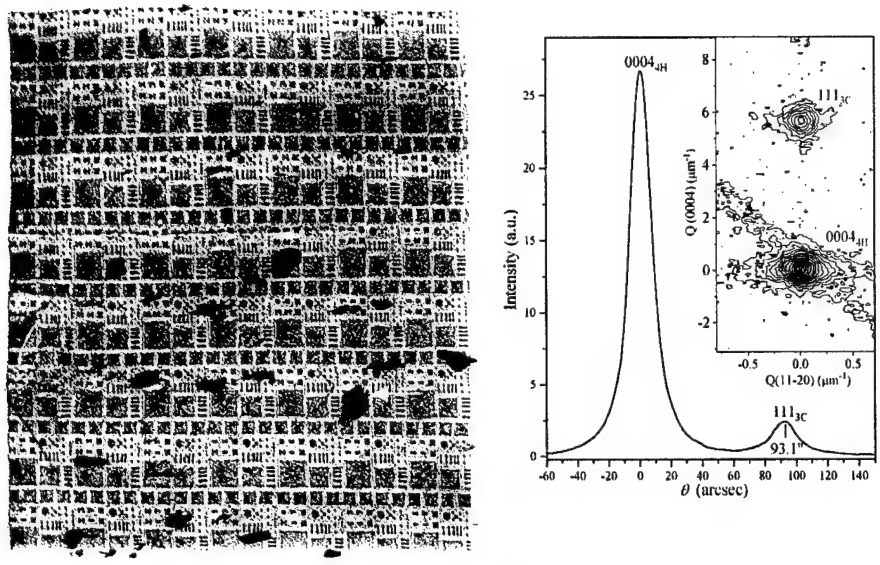

(a) (b)

Fig. 4. (a) Composite image showing the distribution of 3C(I) and 3C(II) (darker regions) in the 3C/4H SiC heteroepitaxial structure. (b) 0004 rocking curve of the arrowed mesa in (a). Cu$K\alpha_1$ radiation. Inset is the triple-axis reciprocal space map, in which the inclined streak on 0004_{4H} is the analyzer streak.

HRTXD study of 3C SiC Epilayer on Isolated 4H SiC flat mesa

The detailed crystalline quality of the 3C-SiC epilayers was investigated by HRXRD. The diffractometer used was a Bede D1 system with two Si (220) channel-cut crystals as the beam conditioner in the four-bounce mode. The conditioned x-ray beam was then limited by a pinhole of 1 mm in diameter. In triple-axis diffraction, a Si (220) channel-cut analyzer was used in the symmetric four-bounce mode. Due to the line-shaped x-ray source, the resulted beam size was larger than the pinhole. By selecting areas with sparse 3C coverage, however, we were able to let the x-ray beam bathe only a single mesa covered by a single 3C variant.

The arrowed mesa in figure 10(a) is a 0.4 × 0.4 mm^2 terrace fully covered by a single-variant 3C epilayer, as indicated by the pure blue color. Figure 4(b) is the 0004 rocking curve taken from this mesa. The substrate peak is very sharp, with the full width at half maximum (FWHM) being 15.3 arcsec, indicating that the mesa contains no dislocation core. Obviously, the well-shaped peak at the right side of the substrate peak is from the epilayer. The FWHM value of this peak is 17.3 arcsec, from which we can estimate that the epilayer thickness is around 0.9 μm. This peak provides further convincing proof that a high-perfection 3C epilayer with macroscopic homogeneity was indeed formed on the mesa studied. The angular separation between the two peaks indicates that the out-of-plane lattice mismatch is $\Delta c/c = -0.14\%$, where c should be understood as the average thickness of the Si-C bilayer ($c_{3C} < c_{4H}$).

To further evaluate the crystalline quality of the 3C-SiC epilayers, we have performed triple-axis diffraction for mesas with well-defined rocking curves. The two-dimensional

$0004_{4H}/0003_{3C}$ reciprocal space map corresponding to the rocking curve in Fig. 4(b) is plotted in the inset, where the upper and lower peaks (spots) are the epilayer and substrate peaks, respectively. Note that in a reciprocal map, the peak spread along the vertical $Q(0004)_{4H}$ direction indicates statistically the extent of the out-of-plane *d*-spacing variation while lattice tilt is reflected by the spread along the horizontal $Q(11\bar{2}0)$ direction. Therefore, the fact that the centers of the two peaks are well aligned on a vertical line (note the patterns corresponding to lattice misorientations in figure 1) shows that there is no misorientation between the epilayer and substrate [*i.e.* the $(0001)_{3C}$ and $(0001)_{4H}$ lattice planes are parallel to each other].

Although the out-of-plane mismatch can be readily calculated as $\Delta c/c \approx -0.14\%$ ($c_{4H} > c_{3C}$) from the symmetric-reflection rocking curve in figure 10(b), the measurement of the in-plane mismatch for 3C/4H heterostructure is difficult. A full examination of reciprocal space shows that $11\bar{2}8_{4H}$ and $11\bar{2}6_{3C}$ (cubic index 402_{3C}) are the only two asymmetric reflections with closely matched Bragg angles. However, in the glancing-exit geometry, it was found that these two peaks are so close to each other that it is difficult to separate them. Rocking curve simulation is also difficult in this case since the diffracting areas of the substrate and epilayer are different. This makes it difficult to use the conventional asymmetric reflection scheme [5] to measure the in-plane mismatch. To overcome this difficulty, we have recently developed a novel diffraction method for absolute lattice parameter measurements with a precision of $10^{-6} \sim 10^{-7}$ Å.

Accurate Lattice Constant and Mismatch Measurements Using Harmonic X-ray Reflections

Measurements of lattice parameters and mismatch by x-ray multiple-order reflections HRXRD is a comparative method mainly used to measure lattice mismatch in heterostructures. In this method, only when the lattice parameter of one component, usually the substrate, is known can one derive the parameters of other components. This limitation arises from a well-known problem in single-crystal x-ray diffraction, *i.e.*, the uncertainty in the zero setting. This uncertainty means that the absolute value of the measured diffraction angle is inaccurate while the only reliable quantity measured is the angular difference. It is this limitation that generally prevents the use of common diffractometers for high-precision lattice parameter measurements.

Therefore, in conventional HRXRD studies of heterostructures, we are in general unable to measure the absolute angular positions of the Bragg peaks. Instead, the deviation of the epilayer diffraction peak from the substrate peak is measured. By assuming that the precise values of the substrate lattice constants are known, one can calculate the absolute Bragg angle of the substrate. Consequently, the absolute position of the epilayer peak may be obtained from its deviation from that of the substrate peak. For largely mismatched heterostructures, or when the epilayer(s) and substrate differ significantly in orientation or crystal symmetry, however, this method usually fails. A typical example is the III-nitride/sapphire heterostructure, where the substrate peak is usually absent in the rocking curves of the nitride film(s). In these cases, measurements of the absolute lattice parameters are required. Unfortunately such measurements cannot be realized with the conventional rocking curve scan.

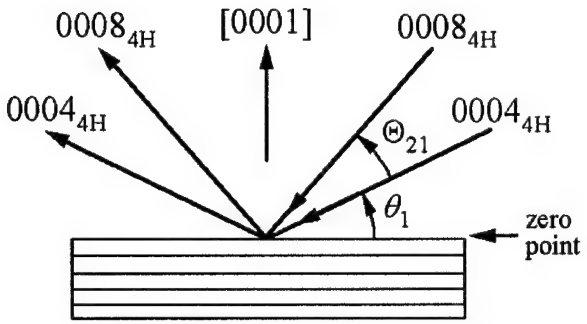

Fig. 5. The relationship between the Bragg angles θ_1 and θ_2 (= $\theta_1 + \Omega_{21}$) of 0004 ad 0008 reflections, respectively, in a wide-range θ–2θ scan.

As the complexity of lattice parameter measurements mainly arises from the uncertainty of the zero setting, here we present a very simple method that is based on multiple-order reflections for solving this problem [6]. The basic principle can be illustrated using the 0004 and 0008 symmetric Bragg reflections of 4H SiC in Fig. 5. Let θ_1 and θ_2 be the Bragg angles of these two reflections. Then the two Bragg equations are

$$2d\sin\theta_1 = \lambda, \qquad (1a)$$

$$2(d/2)\sin\theta_2 = \lambda, \qquad (1b)$$

where d is the spacing of the (0004) lattice planes and λ the x-ray wavelength. In a wide-range θ–2θ scan that covers both Bragg peaks, the measured θ_1 and θ_2 are generally not accurate, but their difference, $\Theta_{21} = \theta_2 - \theta_1$, is an accurate quantity independent of the zero setting. Surprisingly, Eqs. (1a) and (1b) indicate a very simple relationship between Θ_{21} and θ_1:

$$2\sin\theta_1 = \sin(\theta + \Theta_{21}). \qquad (2)$$

Obviously, θ_1 can be numerically solved from Eq. (2) to any precision based on the measured Θ_{21}. Then the true zero point is determined to be $-\theta_1$ relative to 0004 peak. Inserting the calculated θ_1 into Eq. (1a) immediately gives the absolute value of d, provided that λ is known.

From Eqs. (1a) and (2) the measurement precision can be derived as

$$\frac{\Delta d}{d} = \frac{\cot\theta_1 \cos(\theta_1 + \Theta_{21})}{\cos(\theta_1 + \Theta_{21}) - 2\cos\theta_1}\Delta\Theta_{21}. \qquad (3)$$

As an example, the c lattice constant of 4H SiC is roughly 10.08 Å, which gives θ_1 = 17.80° and Θ_{21} = 37.69°, respectively for CuKα1 radiation (λ = 1.540562 Å). The precision of Θ_{21} measured by double-crystal diffractometer is usually in the order of sub-arcsec. If we choose $\Delta\Theta_{21}$ = 0.2", Eq. (3) gives $|\Delta d/d| = 2 \times 10^{-6}$. This is in fact a high

precision (comparable to that of the Bond method) adequate for most applications, and it can be further improved using high-angle reflections (*e.g.* $|\Delta d/d| = 2 \times 10^{-7}$ for Si 333 and 444).

In this method, since the two reflections are activated at the same side of the incident beam, both Bragg peaks have, in principle, symmetric shapes for double- or multi-crystal diffraction. The peak shifts arising from the vertical divergence and the small x-ray refraction effect are largely offset rather than accumulated, although these effects still have to be accounted for if very high accuracy is pursued.

The specimen alignment is almost the same as that in other single-crystal diffraction procedures. In the preferred symmetric Bragg reflection geometry, only the tilt angle χ of the specimen should be carefully adjusted so that the misalignment is minimized within 0.02°. A simple way to achieve this is to adjust χ to make the measured θ_2 angle smallest. When this condition is satisfied, both θ_1 and Ω_{21} are spontaneously minimized.

In addition to lattice parameter measurements, the above method may also be used to measure the x-ray wavelength if it is unknown (usually in synchrotron optics). This simply involves the measurement of the angle Θ_{21} between two multiple-order reflections of a pure Si single crystal (e.g. 220/440 or 333/444). Then based on the computed value of θ_1 and the well-known lattice parameter of Si, the wavelength can be readily calculated from Eq. (2a) to a precision of 10^{-6} Å or less.

Multiple-order reflections have a number of interesting properties and can be used to solve a variety of problems frequently encountered in diffraction physics and x-ray instrumentation. For example, in order to make the lattice parameter measurement reach a precision of $10^{-6} \sim 10^{-7}$, the goniometer is required to have a calibrated angular accuracy of sub-arcsec for rotation ranges of several tens of degrees. Such calibration is generally a very difficult task, but it can be easily realized with multiple-order reflections.

In addition to the 0004 and 0008 reflections of 4H SiC considered above, let us include a third reflection, 0001$\underline{2}$ with a Bragg angle θ_3, in the measurements. Combining the corresponding Bragg equation $2(d/3)\sin\theta_3 = \lambda$ with Eq. (1a) gives another equation

$$3\sin\theta_1 = \sin(\theta + \Theta_{31}), \qquad (4)$$

where $\Theta_{31} = \theta_3 - \theta_1$. Again Θ_{31} can be precisely measured in the $\theta - 2\theta$ scan. On the other hand, using the value of θ_1 obtained from the above measure Θ_{21}, one can actually calculate Θ_{31} from Eq. (4). If the goniometer is accurate, the measured and calculated values of Θ_{31} must be identical [in other words, the zero points determined by the 0004/0008 and 0004/0001$\underline{2}$ reflection pairs should be identical since they both refer to the unique zero point of the (0001) planes]. Otherwise, adjusting the related instrumental parameters (usually of the angular encoders) to make these two values equal can lead to precise calibration of the diffractometer.

The unique advantage of this calibration procedure is that it only involves Eqs. (2) and (4) and is independent of the detailed values of d and λ. Therefore, the calibration is based on a pure geometric effect and may be performed using any reasonable x-ray wavelengths and suitable crystals. The accuracy is not affected by small d-spacing changes arising from homogeneous doping, strains, or thermal expansions. Apparently, this is a very convenient calibration method for x-ray instrumentation and optics.

We have used the novel multiple-order-reflection method to measure the lattice parameter of the high-quality 3C SiC epilayer studied in figure 4. Prior to the measurements, the 0004_{4H}, 0008_{4H} and $00\underline{12}_{4H}$ reflections were used to calibrate the diffractometer. From a wide-range $\theta - 2\theta$ scan, the two Bragg angle differences Ω_{21} and Ω_{31} were carefully measured to be 71505.4" and 174989.5", respectively. These values were well reproducible within an accuracy of 0.5" under stable temperature, but unfortunately they cannot make Eqs. (2) and (4) consistent.

In order to eliminate such a systematic error, a correction factor α is defined to be the ratio between the angle actually rotated and the angle read from the encoder. In defining α, we have assumed that the magnitude of the error is proportional to the rotation angle. Replacing Θ_{21} and Θ_{31} with $\alpha\Theta_{21}$ and $\alpha\Theta_{31}$, respectively, and then taking into account the small refraction corrections, we obtain $\alpha = 1.000563$ from Eqs. (2) and (4). This ratio indicates that without corrections, there will be an angular shortage of 0.563" for a nominal 1000" rotation, which is acceptable for short-range rocking curve scans. For a large-angle rotation of, say 60°, the discrepancy increases to 121.6", which, if not corrected, would be intolerable for lattice parameter measurements. In the following, all the angles referred to are after the α-factor correction.

Only the $0004_{4H}/0003_{3C}$ (cubic index of 0003_{3C} is 111_{3C}) and $0008_{4H}/0006_{3C}$ reflection pairs were chosen for the c lattice parameter measurements (since the 0009_{3C} reflection is extremely weak). During the measurements, the second channel-cut crystal of the monochromator (in the dispersive setting) was carefully adjusted to the CuKα1 peak position and was frequently monitored. Figure 6 shows parts of the $\theta - 2\theta$ scan intensity profile covering these four reflections.

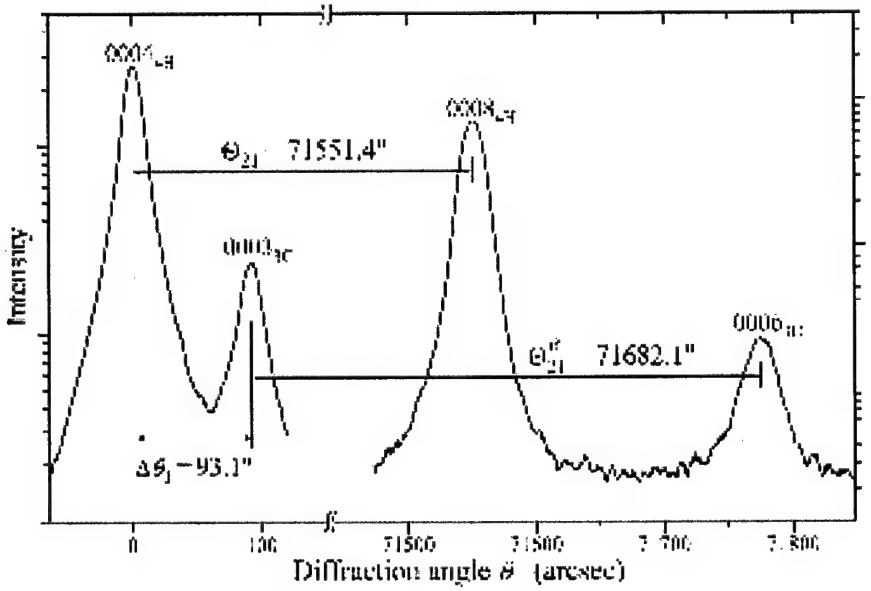

Fig. 6. Rocking curves and peak positions of 0004_{4H} (0003_{3C}) and 0008_{4H} (0003_{3C}) reflections measured from a wide-range θ–2θ scan.

After the refractive-index corrections, the angular distance between 0004_{4H} and 0008_{4H} peaks is Θ_{21} = 71554.5". Then Eqs. (2) and (1a) gives $d = c_{4H}$ = 2.521119 Å. Here c_{4H} represents the average thickness of the Si-C bilayer for 4H-SiC (one fourth of the lattice parameter along [0001]). The corrected angular difference between 0003_{3C} and 0006_{3C} is Θ_{21}^{e} = 71685.2", corresponding to a bilayer thickness of c_{3C} = 2.517586 Å for the 3C epilayer. Thus, the out-of-plane mismatch is $(c_{3C} - c_{4H})/c_{4H} = 1.401 \times 10^{-3}$, which is consistent with the result in figure 10.

In calculating c_{4H} and c_{3C}, we have considered the epilayer and substrate as two independent crystals. Their orientation relationship is actually indicated by the relative positions of the two sets of peaks. In figure 6, because the 0004_{4H} peak is set at $\theta = 0$, the zero points of the epilayer and substrate are $\theta = -\theta_1$ and $\theta = \Delta\theta_1 - \theta_1^e$, respectively, where θ_1^e is the 0003_{3C} Bragg angle and $\Delta\theta_1$ is the splitting between the 0004_{4H} and 0003_{3C} peaks. The difference, $\theta_1 - \theta_1^e + \Delta\theta_1$, obviously represents the misorientation of the epilayer against the substrate. However, the value of this calculated here is less than 0.4", which is negligible, indicating that the 0001_{3C} and 0001_{4H} planes are exactly parallel. This directly confirms an important feature of the growth mechanism designed for the current heteroepitaxy technique, *i.e.*, the 3C SiC epilayer is formed through a two-dimensional layer-by-layer nucleation process on the flat (0001) basal planes rather than the step-flow model commonly dominating SiC growth.

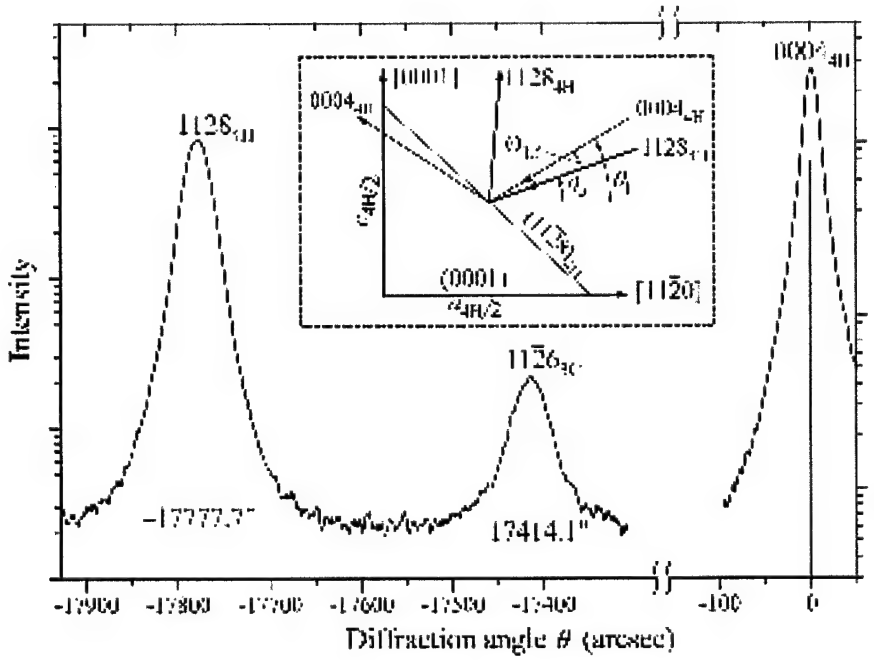

Fig. 7. θ-scan rocking curves of $11\bar{2}8_{4H}$ and $11\bar{2}6_{3C}$ asymmetric reflections relative to the 0004_{4H} Bragg peak. Inset shows the diffraction position of $11\bar{2}8_{4H}$ reflection with respect to that of 0004_{4H}.

After the zero point of the (0001) planes has been determined, the a lattice parameters can be measured with the aid of $11\bar{2}8_{4H}/11\bar{2}6_{3C}$ asymmetric reflections in the glancing-incidence geometry [36]. The relationship between $11\bar{2}8_{4H}$ and 0004_{4H} reflections is illustrated in the inset of figure 7, where the incidence angle of $11\bar{2}8_{4H}$ reflection is $\theta_A = \theta_1 - \Theta_{1A}$. It can be easily proved that the lattice parameter a_{4H} is a function of c_{4H} and θ_A:

$$a_{4H} = \frac{-C_2 + \sqrt{C_2^2 - 4C_1C_3}}{2C_1}, \qquad (6)$$

where $C_1 = c_{4H}\sin\theta_A - \lambda$, $C_2 = c_{4H}^2\cos\theta_A$, and $C_3 = \lambda c_{4H}^2$.

The rocking curves of $11\bar{2}8_{4H}$ and $11\bar{2}6_{3C}$ asymmetric reflections are plotted in figure 13. As the 0004_{4H} peak is located at $\theta = 0$, we have $\Theta_{1A} = 17782.1"$ (after refraction correction), which gives $\theta_A = 46271.3"$. The lattice parameter a_{4H} calculated from Eq. (6) is then 3.07950 Å. Meanwhile, the angular difference between the 0003_{3C} and $11\bar{2}6_{3C}$ peaks is $\Theta_{1A}^e = 17511.6"$ (corresponding to $\theta_A^e = 46634.8"$). Based on the same principle, the basal-plane lattice parameter of the epilayer is calculated as $a_{3C} = 3.08039$ Å. The in-plane mismatch is, hence, $(a_{3C} - a_{4H})/a_{4H} = 2.89 \times 10^{-4}$. Note that in obtaining this parameter, we have successfully avoided the $11\bar{2}8_{4H}/11\bar{2}6_{3C}$ glancing-exit geometry. Although very small, the finite in-plane mismatch clearly shows that the interface of the heterostructure is not perfectly coherent. The cubic lattice of unstrained 3C SiC requires an a/c ratio of $\sqrt{1.5}$ (≈ 1.22474) while the measured ratio is $a_{3C}/c_{3C} = 1.22355$. The difference clearly reveals that the epilayer lattice is compressed in directions parallel to the interface but has a tensile strain along the interface normal. Overall, the epilayer is *partially* relaxed.

Using the multiple-order-reflection method, we have obtained simultaneously but independently two sets of lattice parameters for the two components of the 3C/4H SiC heterostructure. The lattice parameters of 4H SiC measured here are in fact very close to those reported in Refs. [7] and [8].

Although it occasionally suffers a problem that the high orders of a reflection may be inaccessible for long-wavelength radiation, this method is well suited for characterization of most common electronic materials, such as III-V semiconductors, III-nitrides, SiC, etc, with the widely used CuKα1 radiation.

Conclusions

SWBXT is an extremely powerful technique for nondestructive characterization of defects in SiC crystals. Based on the simple geometrical diffraction principle underlying the various imaging processes, it has, to date, provided complete quantitative characterization of both closed-core and hollow-core SSDs as well as other defects, and has provided essential insight into the formation mechanisms of these defects. Being capable of imaging defects in wafers with devices fabricated on them, it has enabled much light to be shed on the influence of the various defects on device performance.

SWBXT is also a simple and efficient technique for identification of SiC polytypes. It has enabled complete polytype determination and variant mapping in 3C/4H and 3C/6H heterostructures, which has significantly facilitated optimization of the growth conditions. In general, SWBXT is an invaluable aid to HRXRD characterization of SiC-based heterostructures that are usually inhomogeneous due to the existence of large number of SSDs and small-angle boundaries in the substrate. SWBXT makes it possible to perform selected area HRXRD measurements, or it can help discern the diffraction contributions of substrate defects in the rocking curves or reciprocal space maps. The combination of SWBXT and HRXRD thus enables us to fully characterize such heterostructures.

Combining these two techniques, we have studied in detail 3C SiC films heteroepitaxially grown on atomically flat mesas on 4H and 6H SiC substrates. These techniques reveal extremely high crystalline perfection and homogeneity of the ideally grown 3C-SiC epilayers on isolated mesas. In particular, the multiple-order-reflection method is successfully applied to measure the absolute lattice parameters of 3C epilayers and 4H and 6H substrates, from which the small strain relaxation effect involved in the heteroepitaxy process is clearly demonstrated. Apart from the small strain relaxation, the 2D nucleation mechanism of the 3C epilayer from a flat coherent interface is clearly revealed from the fact the (0001) lattice planes across the 4H/3C or 6H/3C interface are exactly parallel. These results demonstrate that the "step-free surface heteroepitaxy" growth process is indeed an effective technique for high-quality single-crystal SiC heteroepitaxy.

References

[1] Powell J A, Neudeck P G, Trunek A J, Beheim G M, Matus L G, Hoffman R W and Keys L J 2000 *Appl. Phys. Lett.* **77** 1449

[2] Neudeck P G, Powell J A, Trunek A J, Huang X R and Dudley M 2002 *Mater. Sci. Forum* **389-393** 311

[3] Dudley M, Vetter W M and Neudeck P G 2002 *J. Cryst. Growth* **240** 22

[33] Dudley M, Vetter W M, Huang X R, Neudeck P G and Powell J A 2002 *Mater. Sci. Forum* **389-393** 391

[4] Bowen D K and Tanner B K 1998 *High Resolution X-ray Diffractometry and Topography* (London: Taylor & Francis).

[5] Huang X R, Dudley M, Neudeck P G and Powell J A (to be published)

[6] Fatemi M 2002 *Appl. Phys. Lett.* **80** 936

[7] Tairov Y M and Tsvetkov V F 1983 *Crystal Growth and Characterization of Polytype Structures*, edited by P. Krishna (Oxford: Pergamon Press) pp. 111

[8] Bauer A, Kräußlich J, Dressler L, Kuschnerus P, Wolf J, Goetz K, Käckell P, Furthmüller J and Bechste

2. SWBXT Studies of Langasite and Other Langasite Structure Compounds

This part of the report concentrates on the research carried out on the research project of characterization of the novel piezoelectric resonator crystals langasite ($La_3Ga_5SiO_{14}$ or LGS), langanite ($La_3Ga_{5.5}Nb_{0.5}O_{14}$ or LGN), langatate ($La_3Ga_{5.5}Ta_{0.5}O_{14}$ or LGT) and some newly developed Langasite structure compounds ($Sr_3TaGa_3Si_2O_{14}$ or STGS and etc.). Accompanied with other necessary techniques, such as High Resolution X-ray Diffraction (HRXD), SEM, TEM and Optical Microscopy, SWBXT will be used as the primary investigation technique for the research program.

Background

Resent research showed that langasite ($La_3Ga_5SiO_{14}$ or LGS) and its two isomorphs langanite ($La_3Ga_{5.5}Nb_{0.5}O_{14}$ or LGN) and langatate ($La_3Ga_{5.5}Ta_{0.5}O_{14}$ or LGT) with the $Ga_3Ga_2Ge_4O_{14}$-type structure exhibit piezoelectric properties intermediate between those of quartz and $LiNaO_3$ and $LiTaO_3$. They have temperature compensation at near room temperature, high frequency stability and adequate electromechanical coupling factors for both SAW and BAW devices. Moreover, they also showed that these crystals have very low acoustic friction, which indicates high Q factor. The combination of all these properties, with their high phase transformation temperature and the availability of high quality crystals, makes these crystals currently the most promising piezoelectric materials and useful for a lot of application not only under room temperature but also under high temperature conditions.

It is commonly acknowledged that the performance, yield, reliability and degradation of electric devices, are largely determined by the compositional homogeneity and the presence of defects of the crystals, which the devices are made from. For example, the modification of mode shapes dictates that high quality crystals are required for this technology to reach full potential. Therefore, in order to gain the "perfect" crystals, it is imperative to understand the mechanism of defect generation during crystal growth. Such understanding must be based on the detailed information on the nature and distribution of imperfections in as-grown crystals. Thus, characterization of structural and compositional perfection of the crystal grown is critical to improve the quality and performance of electric devices.

Due to the recent development of new lines of langasite family composition, this part of the research program need to be and, actually, has been extended. And investigation and characterization of new "ordered" langasite structure compounds has been carried out and preliminary results are included here.

Scope of Research

As part of the research program, some specifically emphasized issues to be directly addressed involving all langasite structure compounds, through the development of experiments and theory, include:

- Identification, and development of maps of all of the defects and strains present in crystals of LGS, LGN, LGT and other "ordered" langasite structure crystals grown by various manufacturers;

- Determination of the influence of the various types of defects and strains present in resonators manufactured from the various crystals;

- Provide detailed information on the relationship between growth parameters and defect microstructure.

Results obtained in this research program are likely to provide useful information on the relationship between observed growth defects and growth parameters in these potential resonator crystals and should enable strategy development for crystals' and resonators' quality and performance improvement. Detailed information will also be possibly able to reveal the influence on resonator performance of the various kinds of defect present in the different crystals.

In previous reports we provided a preliminary survey of the quality of langasite, langanite and langatate crystals carried out using SWBXT. Here we report the results of a more systematic study of the defects and strain configuration of LG*X* crystal boules, wafers and resonators. This enables some insight to be gained as to the evolution of the three-dimensional defect microstructure, including the interface shape, during growth.

Data have been obtained from all types of crystals. A selection from these is presented below, following the fabrication procedure of LG*X* crystal devices, i.e., from as-grown LG*X* crystal boules to crystal wafers cut from adjacent locations in the LG*X* boule to resonators made from the wafers.

Preliminary results on the defects content of newly developed "ordered" langasite structure compound STGS were also presented here.

Topography of LGX Boule

First, LG*X* boules were examined by SWBXT in back reflection geometry in order to determine the orientation. Back reflection Laue patterns were recorded. The growth axis of the boules was set to parallel to the incident beam. The diffraction geometry is shown in Fig. 1.

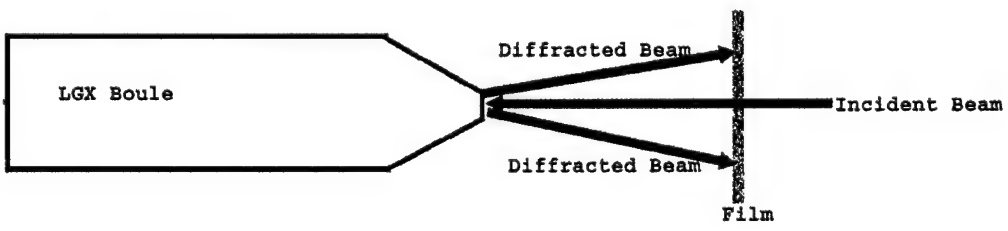

Figure 1. Back reflection geometry

The curved surface of four LG*X* boules, 00-A1-07 LGT-X, 00-A1-08 LGT-X, 01-A4-07 LGN and 00-A4-17 LGT were examined by SWBXT with reflection geometry, shown in Fig. 2.

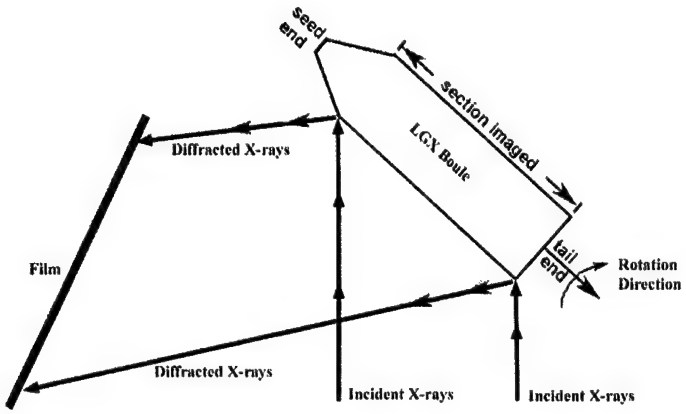

Figure 2. Schematic Diagram of Reflection Geometry

Topographs were recorded covering the entire length of the boules in longitudinal strips. However, the conical surface at the seed end could not be imaged. Only the cylindrical surface with the roughly constant diameter was imaged. After imaging of one strip of surface, the boules were rotated by a few degrees in a clockwise direction (looking at the tail end), the next strip of surface was imaged and the topograph was recorded, until the whole surface was covered. Because of the diffraction geometry utilized, the recorded images suffer considerable distortion, especially along the length of the boule. The magnitude of distortion is different for different reflections and boule position. Accordingly, the lengths of the recorded reflection topographs vary as we rotate the boules. A series of topographs were recorded covering the entire cylindrical surface of the boule. The sequences of topographs are more or less continuous. Some small sections of the surface of the boules were missed due to excess rotation but the overall picture of the boule can still be obtained. The diffraction vector **g** of each topograph is different with each other, while we rotate the boule during the whole imaging process. For all the topographs, **g** vector is approximately pointing axially from the seed end to the tail end, i.e. from left to right on all the topographs shown in here.

Experiment procedure and results of part of each boules are presented and common features are discussed here in detail. Some unique results for each boule will also be discussed.

Total of 36 topographs of the longitudinal surface of each boule were recorded with the method described above. The topographs are recorded starting from 0° (see Fig. 3 and the downward pointing arrow on the optical micrograph, which accompanies each group of topographs), going around the boule as the boule is rotated clockwise.

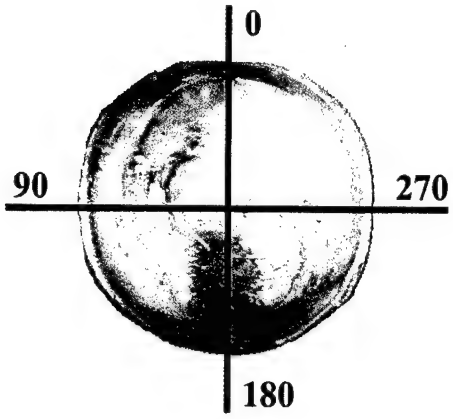

Figure 3. The tail end of the 01-A4-07 LGN boule with the relative rotation angle

Every 9 constituting topographs cover an approximately 90° curved section of the surface of the boule. Topographs were presented in four groups with respect to the corresponding optical micrograph of the boule shown at the bottom of each group of topographs, Fig. 4. Fig. 5 shows an enlargement of topograph II-(b) in the 90° ~ 180° quadrant. And Fig. 6 shows an enlargement of topography III-(b) in the 180° ~ 270° quadrant.

(1) Topographs show well-defined striations K perpendicular to the growth axis X.

(2) Wavy contrast features A are caused by surface ridges running along the length of the boule. These are superimposed onto the striation images (also see I-(e) and I-(f) in 0° ~ 90° quadrant).

(3) Regions of white contrast at the tail end are probably due to the presence of precipitates, P, at the end of growth. Some precipitate type contrast is also visible in the middle sections of the boule.

(4) The several white spots and lines in the middle of the boule, C (not precipitates P), have been created because of the presence of surface projections/depressions, such as small pits, which lead to the situation where no image is locally formation due to blockage of the diffracted beam, Fig. 5.

(5) Vertical white contrast features F are produced in III-(a), III-(b), III-(c) and III-(d) in 180° ~ 270° quadrant, due to risers on faceted steps on the boule (the facets have (0001) orientation) which block the diffracted beam thereby causing bands of white contrast. Where, images can be recorded from the facet itself, smooth surface produces a good quality image and for example, clear striation contrast can be observed, Fig. 6.

Some special features in the other boules:

(1) In boule 01-A4-07 LGN, some white contrast features running across the growth

direction C are due to the heavy ridges going around the boule surface, Fig. 7.

(2) In boule 00-A4-17 LGT, clear wavy surface features due to the ridges running across the boule are superimposed on the well-defined striation contrast, Fig. 8.

(3) In boule 00-A4-17 LGT, vertical white contrast features F due to risers on faceted steps on the boule (the facets have (0001) orientation) which block the diffracted beam thereby causing bands of white contrast, Fig. 9.

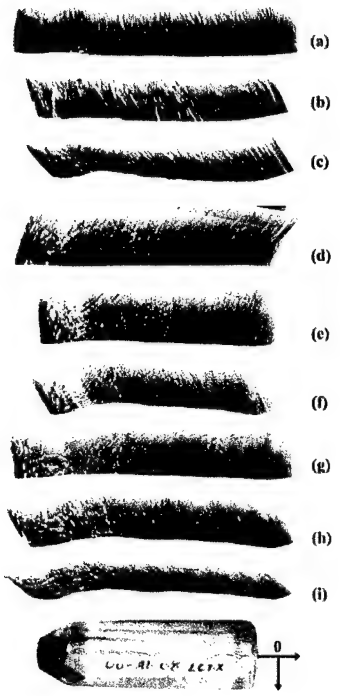

00-A1-08 LGT-X

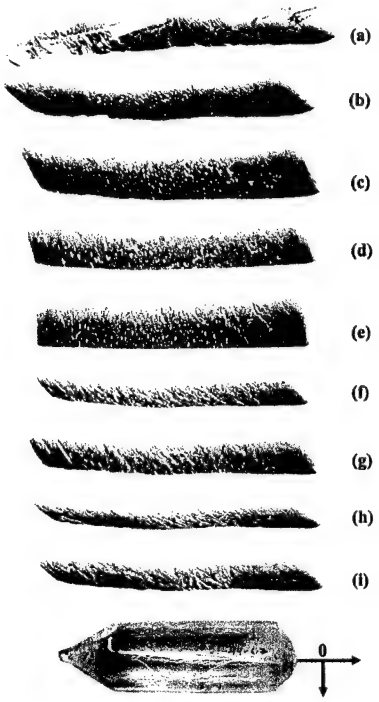

01-A4-07 LGN

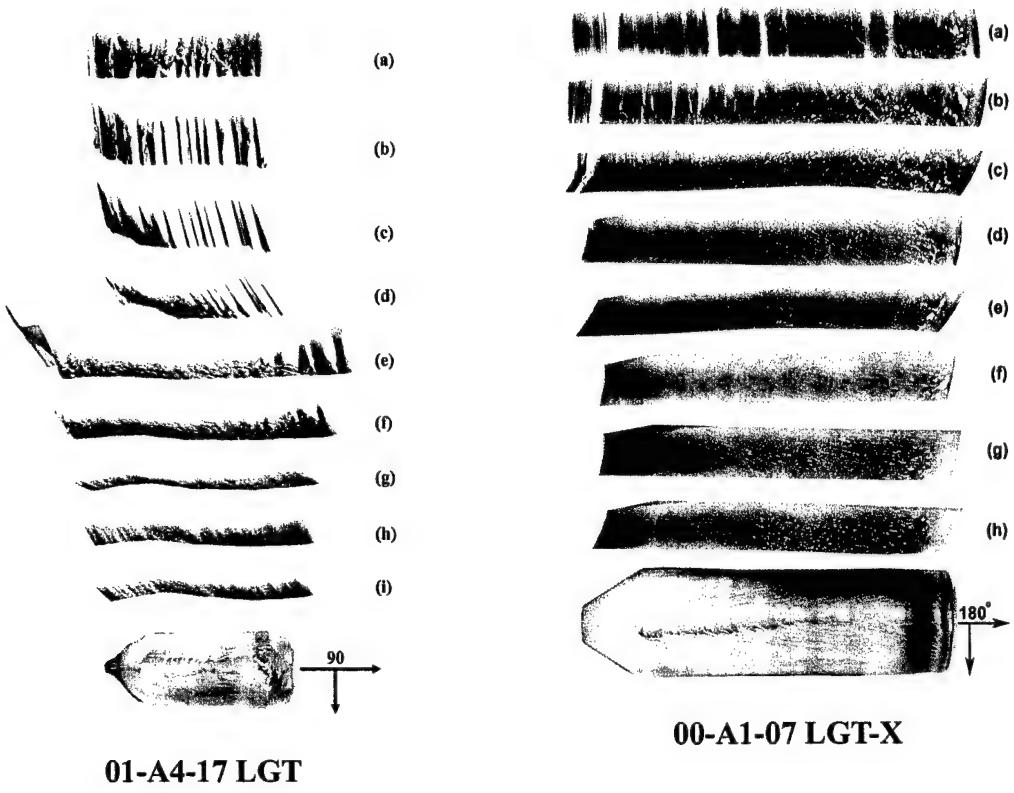

Figure 4. SWBXT images recorded from LG*X* boules

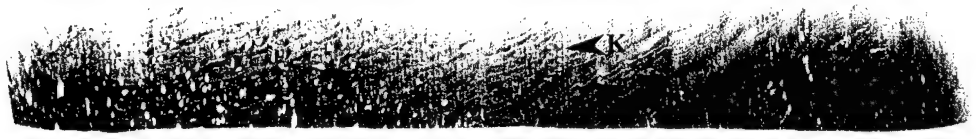

Figure 5. Enlargement of a topograph showing striations, K, precipitates, P, wavy surface feature, A, and rough surface feature C

Figure 6. Enlargement of a topograph showing striation, K, precipitates, P, and facets, F. In this case, striations are clearly shown in the facets

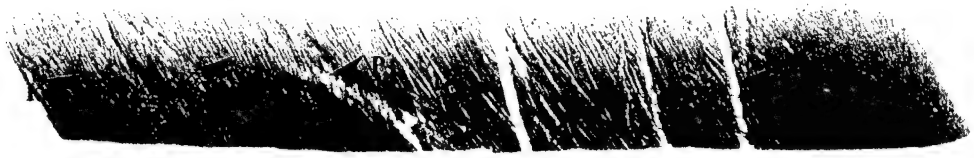

Figure 7. Enlargement of a topograph from 01-A4-07 LGN boule showing the well-defined striations, K, precipitates, P, and wavy surface features, A. White contrasts, C, running across the growth direction are due to the heavy ridges going around the surface

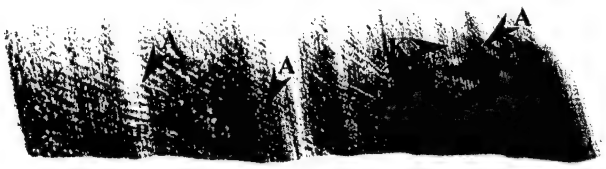

Figure 8. Enlargement of a topograph from 00-A4-17 LGT boule showing that the wavy surface features, A, are superimposed on the well-defined striations contrast, K

Figure 9. Enlargement of a topograph from 00-A4-17 LGT boule, risers on facet steps (with the (0001) orientation) block the diffracted beam thereby causing bands of white contrast F. The smooth surface of the facet produces good striation image K

Topography of LGX Wafers

LG*X* wafers cut from as-grown crystals were examined by SWBXT. Wafers are either Y-cut blanks (cut parallel to the growth axis) or Z-cut blanks (cut perpendicular to the growth axis.

A possible configuration of growth striation rings with growth axis [0001] in LG*X* single crystals is shown in Fig. 10. The possible striation configuration in Y-cut ([001] direction) and Z-cut ([100] direction) are predicted. These predictions were confirmed in this work.

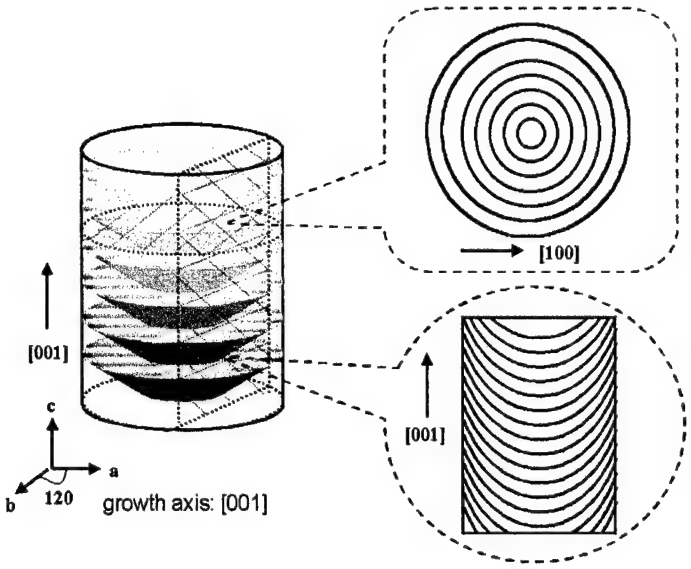

Figure 10. A possible configuration of growth striation rings in LG*X* crystals

Y-cut LGX Wafers

Figure 11(a) shows a transmission topograph recorded from a LGN wafer cut parallel to the [001] growth axis. Well defined contrast of a curved set of striations, K, can be observed in the topograph. Numerous band-like nearly white contrast segments, D, are likely to be dislocations running through the wafer from bottom to top; the one very long segment is likely to be a group of growth dislocations running at a small angle to the growth axis. Some surface artifacts and scratches, S, can be observed. Precipitates or inclusions, P, are evenly distributed throughout the whole sample. And some linear row of inclusions, I, can also be discerned.

Figure 11(b) shows a transmission topograph recorded from a LGT wafer cut parallel to the [001] growth axis. Weak contrast of a curved set of striations, K, can be observed in the topograph. Same band-like white contrast segments, D, can be observed. The one very long segment, also noted as D, is likely to be a group of growth dislocations running at a small angle to the growth axis. Some surface artifacts, A, can be observed in the wafer. There are no precipitates or inclusions can be discerned.

Compare with topograph of the Y-cut LGN wafer in Figure 11(a), the weaker contrast from striations and dislocations in Figure 11(b) may be attributed to:

(1) poor inherent crystal quality and/or

(2) poor surface finish.

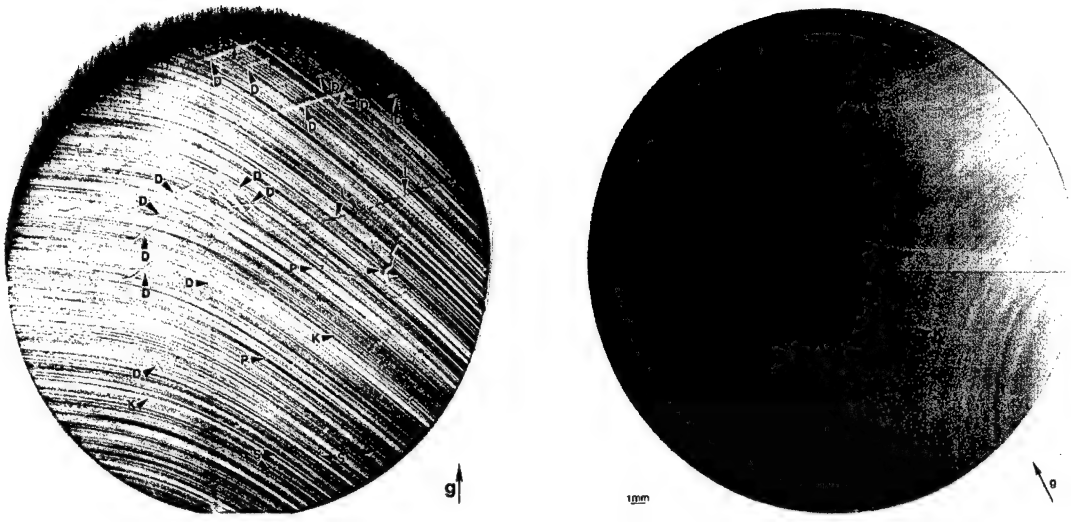

(a) A Y-cut LGN wafer **g** = 0002 (b) A Y-cut LGT wafer **g** = $\bar{1}100$

Figure 11. Transmission topographs recorded from two Y-cut LG*X* wafers

X-cut LGX Wafers

A series of Z-cut wafers cutting from a same LGT boule at continuous position were under investigation by SWBXT. Topographs were recorded in transmission geometry, Fig. 12. These series images, although may not be in the right sequence due to the lack of information, give out the "snapshots" of the local interface shape in the wafer volume. Slight modifications were observed from wafer to wafer, reflecting the evolution of interfaces shape during the crystal growth.

In these topographs, the well-defined contrast of concentric striation rings were clearly shown. The concentric striations indicate and prove that the growth interface is either concave or convex, rather than flat; and indicate the presence of slight lattice parameter fluctuations during the crystal growth process. This again confirms that the configurations giving rise to the formation of the concentric striation rings shown in Fig. 10 is highly possible during crystal growth. The spacing of the concentric striation rings reveals the periodicity of the striations, which indicates the periodicity of fluctuations during growth. The concentric striation rings are not quite symmetric which reveals an asymmetry in the thermal field inside the growth chamber.

Note in the core region of the wafers, Fig. 13(a), irregular striation rings in the center of the crystal indicate uneven growth near the core of the crystal; possible interface breakdown close to the crystal core is also observed, along with the attendant inhomogeneous distortion. The asymmetry of the interface shape in the central region is apparently propagated throughout the crystal.

Dislocation slip bands that appear to originate from the inhomogeneous distortion

generated by the irregular interface shape are visible as several bands marked as B running across the middle section of the sample, Fig. 13(b). In all wafers, the central region is invariably surrounded by slip bands and generally is the region with highest dislocation density, further emphasizing the lower crystal quality in this region. These slip bands are possibly generated by the thermal stresses, which accompany the irregular interface shape and growth in this region.

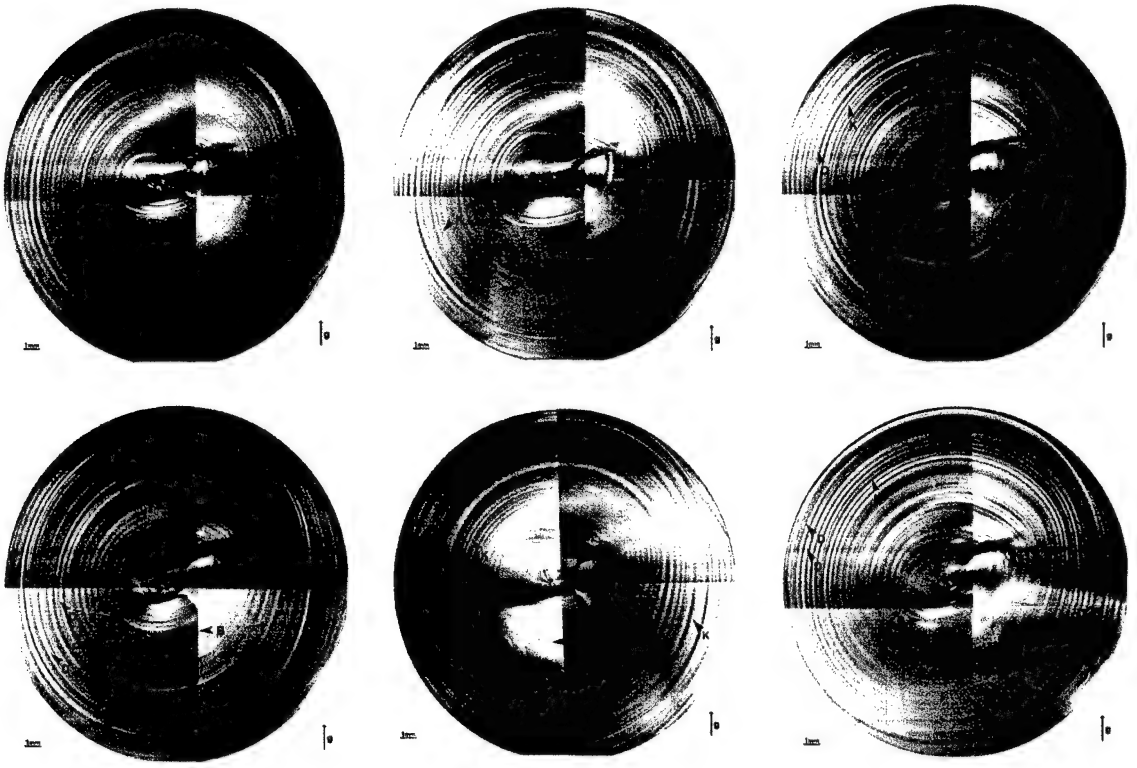

Figure 12. Transmission topographs recorded from a series of Z-cut wafers from one LGT boule

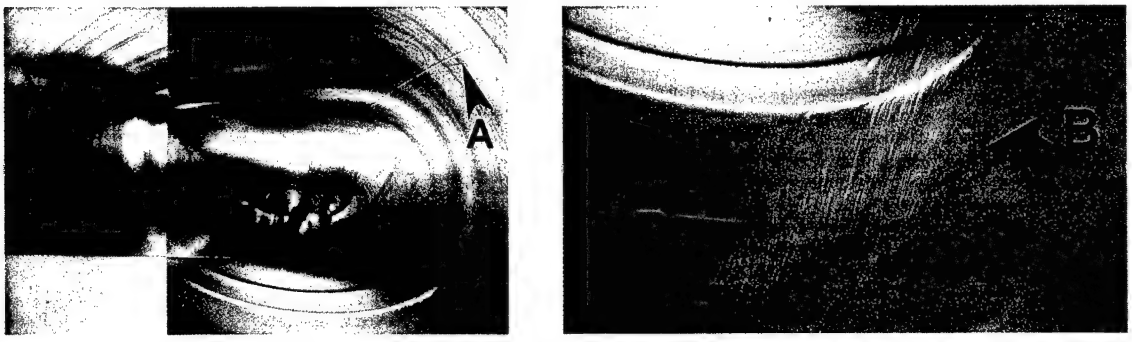

(a) Detail of the core region (b) Slip bands surrounding the core region

Figure 13. Enlargement of the core region and the surrounding slip bands

Precipitates or inclusions can be observed in every sample. They are mainly distributed around the core area (Fig. 13, white spots with different size), providing the further evidence of inhomogeneous growth in the core region

Numerous band-like nearly white contrast segments, likely to be dislocations, run through the wafer from bottom to top, Fig. 14.

Figure 14. Dislocation-like contrast in LGT wafers

Topography of LGX Resonators

Topographs recorded with resonators fabricated from two different LGN crystal boules. Two of the topographs, one from each LGN-4 and LGN-8 boules, are shown in Fig. 15(a) and Fig. 15(b) respectively.

Compare the resonators made from both LGN-4 and LGN-8 boules:

(1) Well-defined sets of striations K can be observed in all resonators from both boules. However, the striation contrast visible on wafers cut from boule LGN-4 was much sharper and more well-defined than that visible on wafers cut from LGN-8.

(2) Strain contrast associated with the edge of the electrode superimposed on the striation contrast.

(3) Surface dominant contrast associated with the interaction between LGN sample surface and the electrode can be observed in all images.

(4) In the set of resonators cut from LGN-8, there are regions where the interface shape becomes grossly distorted. In those regions, the clarity of the striation images is further reduced. This indicates the differences in growth conditions or control for LGN-8 compared to LGN-4, and that the general quality of LGN-8 wafers is inferior to those from LGN-4.

(5) The interface distortion visible in LGN-8 wafers provides some evidence in favor of poorer inherent crystal quality. Further insight into the relative importance of these two possible contributory factors could be determined by further studies carried out with High Resolution X-ray Diffractometry and further SWBXT studies carried out after repolishing the crystals.

(6) Clear images of dislocations and inclusions are also observed on LGN-4 wafers but not on LGN-8 wafers. The poorer contrast obtained from LGN-8 wafers may arise from: poor inherent crystal quality (compared to LGN-4) and/or poor surface finish.

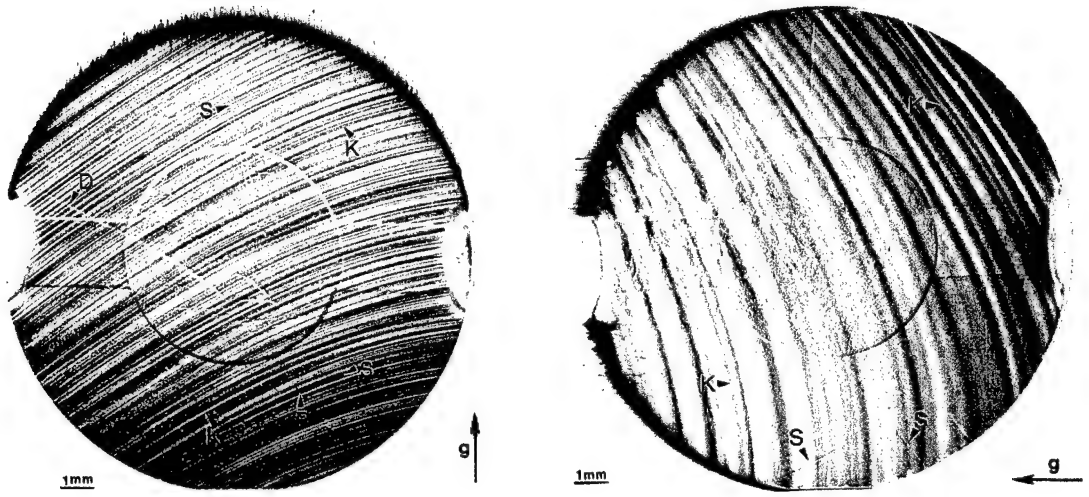

(a) From LGN-4 crystal (b) From LGN-8 crystal

Figure 15. Transmission topographs recorded from LGN resonators

The attempt to correlate the LGN resonator mcirostructures with Q•f factors has been carried out. However, all the resonators examined (from two different boules) had striations present, so the effect of striations on Q•f could not be assessed directly. However, the surface quality of wafers from one boule was better than the other, might suggest a possible correlation.

Topography of STGS Boule

As the further development of research on LGS, LGN and LGT, two major disadvantages of those materials have been perceived. First, high Ga_2O_3 content among the raw materials makes the crystal cost much higher than quartz, $LiNbO_3$ and $LiTaO_3$. Second, more importantly, the crystal structure of these compounds is "disordered". The "disordering" results primarily from the fact that two of the cations in each compounds randomly share the same sites in the unit cell, for LGS, Ga^{3+} and Si^{4+} sharing the same two small tetrahedral sites; for LGT and LGN, the Ga^{3+} and Ta^{5+} or Ga^{3+} and Nb^{5+} sharing the same single octahedral sites. This causes randomly distributed distortion to

the crystal structure, affecting the material uniformity and reproducibility and leading to lower than ideally achievable acoustic Q and electromachanical coupling.

Based on the "order-disorder" argument, several completely "ordered" langasite structure compounds have been developed, including $Sr_3TaGa_3Si_2O_{14}$ or STGS, $Ca_3TaGa_3Si_2O_{14}$ or CTGS, $Sr_3NbGa_3Si_2O_{14}$ or SNGS and $Ca_3NbGa_3Si_2O_{14}$ or CNGS. Here, preliminary SWBXT results of STGS boule are presented.

An as-grown crystal of STGS was examined by SWBXT in the same way as the other four LG*X* boules. Fig. 16 shows the tail and seed end of the boule.

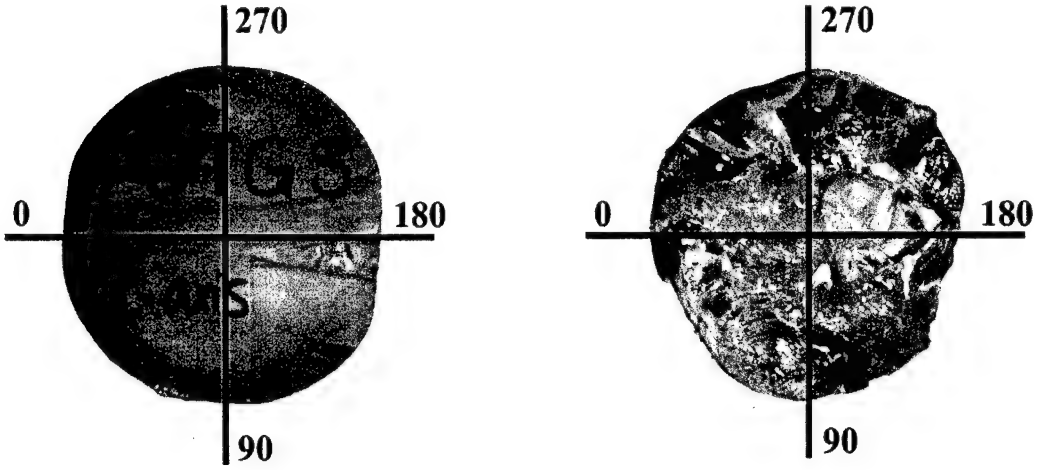

Figure 16. The tail and seed end of the STGS boule with the relative rotation angle positions.

Part of the topographs were presented, as before, in two groups with respect to the corresponding optical micrograph of the boule shown at the bottom of each group of topographs, Fig. 2-15. There are no clear striation contrasts which can be observed in most of the topographs. Wavy contrast features, A, are caused by the ridges on the surface running along the length of the boule. Possible precipitate contrasts, P, can be observed throughout the whole boule. And other contrast due to surface roughness can also be observed.

This new STGS crystal tend to have very strong facet formation during crystal growth.Vertical white contrast features, F, observed in 90° ~ 180° and 180° ~ 270° quadrants, are produced by facet risers with the same formation mechanism as before in other LG*X* crystals. Some striation-like contrast can be observed in the facet area, but, in this case, it is not clear if it is from striations or due to surface features (Fig. 17). The enlarged topograph (i) in 90° ~ 180° quadrant, Fig. 18, clearly show this unique contrast feature differentiating between LGN and LGT crystals.

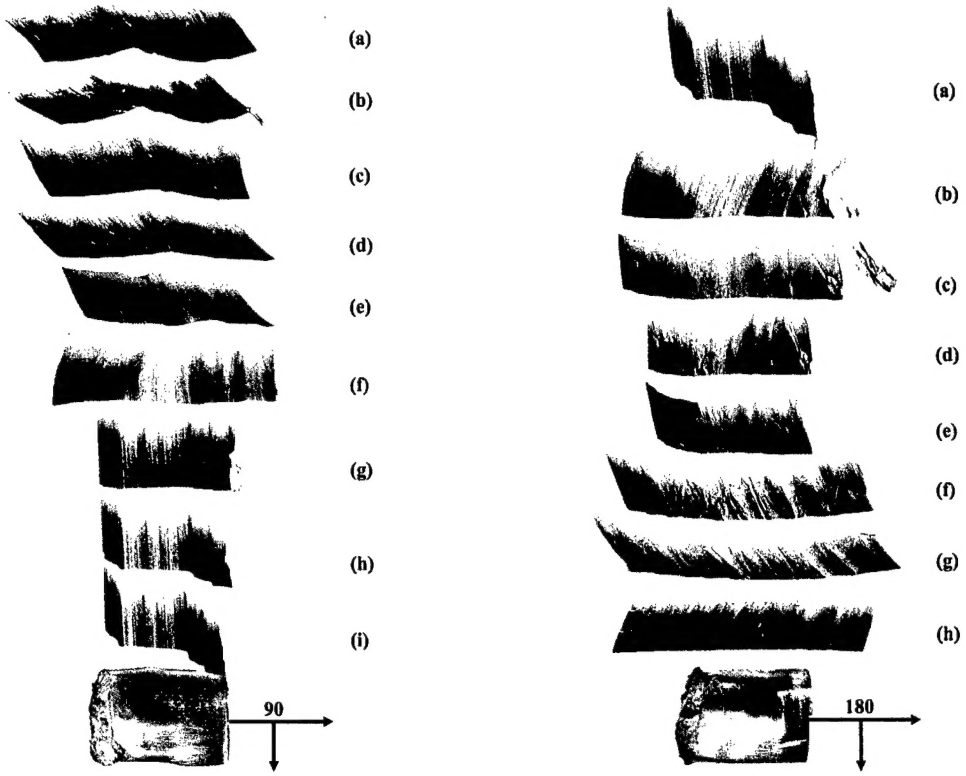

Figure 17. SWBXT images recorded from STGS boule

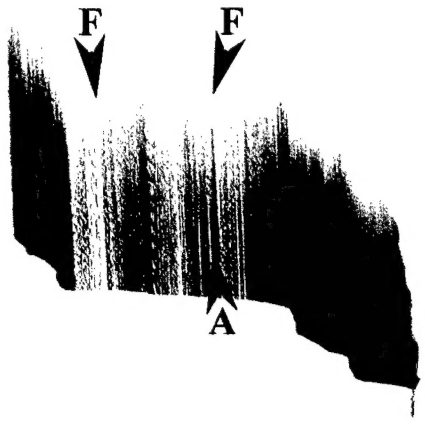

Figure 18. Enlargement of topograph (i) in 90° ~ 180° quadrant showing wavy surface feature, A, and vertical white contrast facet features, F, along with some striation-like contrast

Discussion: Striations in LGX Crystals

1. Striations are the most significant defects in LG*X* crystal growth.

2. In LG*X*, the striations are not visible optically. And there is no report of striations

revealing in LG*X* by chemical etching or other techniques. The presence of striations was only revealed by X-ray topography, so far.

3. In LG*X*, the striations originate due compositional variations or non-stoichiometry in the melt. These can arise due to:

   a. the small size or even absence of the field of congruent melting (where the melt composition is the same as the solid), due to the complexity of the ternary component system (e.g. La_2O_3 - Ga_2O_3 - SiO_2);

   b. small but finite evaporation of Ga_2O_3 from the melt.

4. This non-stoichiometry in the melt can also give rise to the effect of constitutional supercooling, which can drive interface breakdown or cellular growth. SWBXT images of LGN wafers cut perpendicular to the growth axis give out strong evidence.

5. To prevent striations, some possible ways are:

   a. carefully prepare starting melt composition;

   b. improve temperature control, keep growing proceed at a most exactly stoichiometric melt composition;

   c. reduce temperature fluctuation during crystal growth;

   d. reduce evaporation by improving the growth atmosphere.

Discussion: Assessing the Influence of Striations

1. Generally, in order for defects to significantly affect the Q factor, they must have some internal movement that does not respond instantaneously to an applied stress. They must be anelastic; as, for example, point defects with thermally activated relaxations between orientations and dislocations that bow out non-instantaneously in response to stress.

2. Since striations are associated with slight variations in crystal structure (variations in composition and lattice spacing), they will result in spatial variations of the elastic constants. However, they will not necessarily have an anelastic response to acoustic waves and, therefore, may not affect the Q factor. This depends on whether applied stress induces a slight restructuring of the atoms in the striations. So, a lack of effect on Q factor is possible.

3. On the other hand, it would be surprising if striations had no effect on the temperature independence of oscillators. Local variations of elastic constants are bound to produce changes in the bulk elastic constants (at wavelengths long compared to the periodicity of the striations) and their temperature derivatives.

In addition, the effects can be expected to be different for different elastic constants, since striations have a directionality.

Conclusions

Systematic SWBXT studies have been carried out of LGX and STGS wafers and boules. This enables the overall three-dimensional distribution of defects and strains to be determined. The boule images revealed growth striations and precipitates. Wafers cut parallel to the growth axis enable insight into the evolution of the interface shape during growth. Significant irregularities were observed. Imaging of wafers cut perpendicular to the growth axis confirmed the irregularities in interface shape, and provided clear views of the highly irregular interface shape in the central region of crystal. This regions was found to be highly strained to the point where dislocation generation was visible. The detailed origins of the striations have not yet been determined, i.e., the exact nature of the deviations from stoichiometry. Further studies are underway.

REFERENCES

1. B. Chai, J. L. Lefaucheur, Y. Y. Ji and H. Qiu, Proceedings of the IEEE International Frequency Control Symposium, 1998, 748

2. J. Hornsteiner, E. Born, G. Fischerauer and E. Riha, Proceedings of the IEEE International Frequency Control Symposium, 1998, 615

3. A. N. Gotalskaya, D. I. Drezin, V. V. Bezdelkin and V. N. Stassevich, Proceedings of the IEEE International Frequency Control Symposium, 1993, 339

4. R. C. Smythe, Proceedings of the IEEE International Frequency Control Symposium, 1998, 761

5. J. Detaint, J. Schwartzel, A. Zarka, B. Capelle, J. P. Denis and E. Philippot, Proceedings of the IEEE International Frequency Control Symposium, 1994, 58

6. H. Fritze, H. L. Tuller, H. She and G. Borchardt, Sensors and Actuators B, **76**, 103, (2001)

7. H. Fritze and H. L. Tuller, Appl. Physics Letters, **78**, 976, (2001)

8. R. C. Smythe, R. C. Ilelrnbold, G. E. Hague, II, and K. A. Snow, IEEE Transactions on Ultrasonics, Ferroelectrics, and Frequency Control, **47**, 355, (2000)

9. S. Park and D. A. Keszler, Solid State Sciences, **4**, 799, (2002)

10. B. V. Mill and M. V. Lomonosov, Proceedings of the IEEE International Frequency Control Symposium and PDA Exhibition, 2001, 255

11. B. H. T. Chai, A. N. P. Bustamante and M. C. Chou, Proceedings of the IEEE/EIA International Frequency Control Symposium and Exhibition, 2000, 163

TECHNOLOGY TRANSFER

Strong interaction has occurred with Dr. Phil Neudeck of NASA Lewis Research Center, and Dr. Christian Fazi, and S. Tiddrow of U.S. Army Research Laboratory, Adelphi. Interactions have also occurred with the major SiC crystal manufacturers Cree Research, Inc., ATMI, and Sterling Semiconductor (although these interactions are also separately funded). Preliminary interactions have been initiated with Crystal Photonics Inc., a manufacturer of the piezoelectric crystals, and with Christine Klemenz of University of Central Florida, who is growing thin films of the materials.